Monthly Notices
of the
ROYAL ASTRONOMICAL SOCIETY

MNRAS **449,** 2937–2973 (2015) doi:10.1093/mnras/stv349

A comprehensive *HST BVI* catalogue of star clusters in five Hickson compact groups of galaxies

K. Fedotov,[1,2⋆] S. C. Gallagher,[1] P. R. Durrell,[3] N. Bastian,[4] I. S. Konstantopoulos,[5] J. Charlton,[6] K. E. Johnson[7] and R. Chandar[8]

[1] *University of Western Ontario, London, ON N6A 3K7, Canada*
[2] *Herzberg Institute of Astrophysics, National Research Council of Canada, Victoria, BC V9E 2E7, Canada*
[3] *Department of Physics and Astronomy, Youngstown State University, Youngstown, OH 44555, USA*
[4] *Astrophysics Research Institute, Liverpool John Moores University, Liverpool L3 5RF, UK*
[5] *Australian Astronomical Observatory, North Ryde, NSW 1670, Australia*
[6] *Pennsylvania State University, University Park, PA 16802, USA*
[7] *Department of Astronomy, University of Virginia, Charlottesville, VA 22904, USA*
[8] *Department of Physics and Astronomy, University of Toledo, Toledo, OH 43606, USA*

Accepted 2015 February 13. Received 2015 February 13; in original form 2014 October 15

ABSTRACT

We present a photometric catalogue of star cluster candidates in Hickson compact groups (HCGs) 7, 31, 42, 59, and 92, based on observations with the Advanced Camera for Surveys and the Wide Field Camera 3 on the *Hubble Space Telescope*. The catalogue contains precise cluster positions (right ascension and declination), magnitudes, and colours in the *BVI* filters. The number of detected sources ranges from 2200 to 5600 per group, from which we construct the high-confidence sample by applying a number of criteria designed to reduce foreground and background contaminants. Furthermore, the high-confidence cluster candidates for each of the 16 galaxies in our sample are split into two subpopulations: one that may contain young star clusters and one that is dominated by globular older clusters. The ratio of young star cluster to globular cluster candidates varies from group to group, from equal numbers to the extreme of HCG 31 which has a ratio of 8 to 1, due to a recent starburst induced by interactions in the group. We find that the number of blue clusters with $M_V < -9$ correlates well with the current star formation rate in an individual galaxy, while the number of globular cluster candidates with $M_V < -7.8$ correlates well (though with large scatter) with the stellar mass. Analyses of the high-confidence sample presented in this paper show that star clusters can be successfully used to infer the gross star formation history of the host groups and therefore determine their placement in a proposed evolutionary sequence for compact galaxy groups.

Key words: galaxies: evolution – galaxies: groups: general – galaxies: interactions – galaxies: star clusters: general.

1 INTRODUCTION

It is widely accepted that interactions and mergers between gas-rich galaxies lead to star formation (e.g. Kennicutt et al. 1987; Mihos & Hernquist 1996; Barton Gillespie, Geller & Kenyon 2003; Springel, Di Matteo & Hernquist 2005), and that the majority of stars form in clusters and associations (Lada & Lada 2003; Bressert et al. 2010). It therefore follows that a detailed analysis of star cluster (SC) populations in a galaxy can reveal its history of interaction events (e.g. Whitmore et al. 1999; Gallagher et al. 2001; Bastian et al. 2005; Wilson et al. 2006).

In that light, SCs are a powerful tool for studying star formation events triggered by mergers and tidal interactions between galaxies. In particular, SCs could prove useful for studying compact groups (CGs), specifically Hickson Compact Groups (HCGs; Hickson 1982, 1997; Hickson, Kindl & Auman 1989; Hickson et al. 1992). By virtue of their selection criteria (low velocity dispersions and high galaxy number densities), HCGs represent an environment with frequent and prolonged interactions, that can trigger the formation of SC populations associated with specific events.

Initially motivated by the work of Verdes-Montenegro et al. (2001), Johnson et al. (2007) proposed an evolutionary sequence of HCGs by separating them into three types based on the ratio of their H I content (a proxy for the available reservoir of cool gas for

⋆ E-mail: kfedotov@uwo.ca

Table 1. Details of observations.

Group	Galaxy	Instrument	Programme ID	t_{exp} (s)			Date	References
				*F*435*W**	*F*606*W*	*F*814*W*		
HCG 07	A, B, D	ACS/WFC	10787	1710	1230	1065	2006 Sept	K10
	C	ACS/WFC		1710	1230	1065	2006 Sept	
HCG 31	A–C, E–H	ACS/WFC	10787	1710	1230	1065	2006 Aug	G10
HCG 42	A, C	ACS/WFC	10787	1710	1230	1080	2007 Dec	K13
HCG 59	A, C	ACS/WFC	10787	1710	1230	1065	2007 Dec	K12
	B, I	ACS/WFC		1710	1230	1065	2006 Nov	
HCG 92	B, D	WFC3	11502	3410	1395	1860	2009 Aug	F11, T12
	C, B	WFC3		3410	1395	1860	2009 Aug	
	E	WFC3		3410	1395	1860	2009 July	

Notes. *For HCG 92 B filter is *F*438*W* of WCF3 camera. In the last column we reference SC studies that used the associated observations.
G10: Gallagher et al. (2010)
F11: Fedotov et al. (2011)
K10: Konstantopoulos et al. (2010)
K12: Konstantopoulos et al. (2012)
K13: Konstantopoulos et al. (2013)
T12: Trancho et al. (2012).

star formation) and the dynamical mass,[1] with Type I being the gas-rich groups and Type III the gas-poor ones. Johnson et al. (2007) also report – based on *Spitzer* mid-infrared colours – that galaxies in Type I groups are more actively star-forming than galaxies in Type II groups while galaxies in Type III groups are relatively quiescent. Konstantopoulos et al. (2010) expanded on this classification by splitting group types into two parallel sequences according to their gas distributions: Sequence A groups maintain the bulk of their cold gas inside galaxies, whereas Sequence B groups have gas dispersed throughout the intragroup medium (IGM; Konstantopoulos et al. 2010, their fig. 1). The gas distribution of Sequence B groups likely results from strong interactions that occur while disc galaxies are still gas-rich. The initial conditions of the positions and relative velocities of Sequence A group galaxies are such that only softer interactions occur, and while secular evolution may be enhanced and lead to a boost in star formation rates (SFRs) in individual galaxies, the bulk of the cold gas is not pulled into the IGM. As a consequence, the groups in Sequence A are expected to ultimately lead to the formation of a single elliptical galaxy with little to no X-ray envelope, as gas is consumed within galaxies before late-stage dry mergers. Groups in Sequence B – where galaxies interact strongly before gas is consumed – would be more likely to form ellipticals with a strong X-ray envelope (heated by star formation triggered by one or more gas-rich mergers), as can be seen around some massive elliptical galaxies or so-called fossil groups (Jones et al. 2003). The differences in star-forming histories, which vary depending on gas content and distribution and advance along the evolutionary path, must be reflected in the SC populations of the groups. Thus, SC populations can potentially be used to infer their hosts' placement on the CG evolutionary sequence proposed by Konstantopoulos et al. (2010).

In this paper, we consolidate the information on SCs in CGs of galaxies that has been presented in a number of projects (Gallagher et al. 2010; Konstantopoulos et al. 2010, 2012, 2013; Fedotov et al. 2011) and present it in a consistent, coherent catalogue, with the goal of further assisting researchers in SC-related studies. We also take this opportunity to compare the basic properties between cluster populations in CGs at distinct evolutionary stages.

This paper is organized in the following way. In Section 2, we describe the samples and data sets. We outline the procedure for constructing the catalogue in Section 3, and present our results and discuss them in Section 4. Lastly, we summarize the main conclusions in Section 5. Throughout, we use the cosmology $H_0 = 73.0$ km s^{-1} Mpc^{-1}, $\Omega_{matter} = 0.27$, and $\Omega_{vacuum} = 0.73$ to determine distances and physical sizes.

2 DATA

The data for this project were obtained with the *Hubble Space Telescope* (*HST*) Advanced Camera for Surveys (ACS) and Wide Field Camera 3 (WFC3). These observations are part of two programmes: ID 10787 (PI J. Charlton) and ID 11502 (PI K. Noll). The observations were carried out in the *F*435*W* (*F*438*W* for WFC3), *F*606*W*, and *F*814*W* filters, which are similar to the Johnson *BVI* bands. Hereafter, we refer to the *HST* filters as B_{435}, B_{438}, V_{606}, and I_{814}, although we did not make transformations to the Johnson–Cousins system.

Table 1 contains an observation log. The last column in the table lists publications related to those observations. Table 2 presents properties of the 16 individual galaxies within the five CGs included in this sample.

3 DATA ANALYSIS

Before we go into the detailed description of selecting and sorting the detected sources, here are a few words about our terminology to clarify the differences between samples.

Our catalogue consists of all detected point sources that passed the criteria described below. However, the high-confidence portion of the catalogue is divided into two subcategories that we denote as star cluster candidates (SCCs) and globular cluster candidates (GCCs). The major difference between these two subcategories is that the selection criteria for the SCCs does not discriminate against sources with significant nebular emission. In contrast, the selection criteria for GCCs filter out objects with nebular emission (both in

[1] Alternative dynamical classifications exist that determine the state of the group through means other than mass ratios. For example, Bitsakis et al. (2011) use early-type galaxy fractions to ascertain the dynamical state of a group.

Table 2. HCG galaxies information.

Galaxy	Name	RA (2000)	Dec. (2000)	Type	v_r (km s^{-1})	M_* log ($M_\odot$)	SFR ($M_\odot$ yr^{-1})
07A	NGC0192	$00^h39^m13.^s4$	$+00°51'52''$	Sb	4133	11.28	3.88 ± 0.47
07B	NGC0196	$00^h39^m17.^s8$	$+00°54'46''$	SB0	4255	10.76	0.23 ± 0.02
07C	NGC0201	$00^h39^m34.^s8$	$+00°51'36''$	SBc	4415	10.89	2.06 ± 0.17
07D	NGC0197	$00^h39^m18.^s8$	$+00°53'31''$	SBc[a]	4121	10.15	0.43 ± 0.04
31A	NGC1741	$05^h01^m38.^s7$	$-04°15'34''$	Sdm	4074[b]	10.32[c]	8.11 ± 0.74[c]
31B		$05^h01^m36.^s2$	$-04°15'43''$	Sm	4136[b]	9.51	0.78 ± 0.07
31C	M1089	$05^h01^m37.^s7$	$-04°15'28''$	Im	4019[b]	[c]	[d]
31E		$05^h01^m37.^s5$	$-04°15'57''$	Sdm	4009[e]	–	[d]
31F		$05^h01^m40.^s0$	$-04°16'22''$	Sbc	3969[e]	–	0.19 ± 0.02
31G	IC 0399	$05^h01^m44.^s0$	$-04°17'20''$	Sbc	3991	10.04	1.47 ± 0.12
42A	NGC3091	$10^h00^m14.^s3$	$-19°38'13''$	E3	3964	11.53	0.44 ± 0.04
42C		$10^h00^m10.^s3$	$-19°37'19''$	E2	4005	10.70	0.09 ± 0.02
59A	IC 0737	$11^h48^m27.^s5$	$+12°43'39''$	Sa[f]	4109	10.19	4.99 ± 0.67
59B	IC 0736	$11^h48^m20.^s1$	$+12°43'00''$	E0[g]	4004	10.14	0.02 ± 0.01
59C	KUG 1145+129	$11^h48^m32.^s4$	$+12°42'19''$	Sb	4394	9.82	0.16 ± 0.03
59D	KUG 1145+130	$11^h48^m30.^s6$	$+12°43'47''$	Im	3635	9.38	0.48 ± 0.04
92B	NGC7318B	$22^h35^m58.^s4$	$+33°57'57''$	Sbc	5774	10.89	0.52 ± 0.01[h]
92C	NGC7319	$22^h36^m03.^s5$	$+33°58'33''$	SBc	6747	11.35	0.08 ± 0.05[h]
92D	NGC7318A	$22^h35^m56.^s7$	$+33°57'56''$	E2	6630	11.19	0.05 ± 0.01[h]
92E	NGC7317	$22^h35^m51.^s9$	$+33°56'42''$	E4	6599	10.83	0.03 ± 0.01[h]

Notes. Unless indicated otherwise stellar masses taken from Desjardins et al. (2014), SFR values listed are from Tzanavaris et al. (2010), velocity values from de Vaucouleurs et al. (1991), and morphology types from Hickson et al. (1989).
[a]In RC3 galaxy listed as SB0.
[b]Nishiura et al. (2000).
[c]Stellar mass value listed is measured as the total mass of galaxies 31A and 31C.
[d]SFR value listed is combined value of galaxies 31A, 31C, and 31E.
[e]Mendes de Oliveira et al. (2006).
[f]In RC3 galaxy listed as E?.
[g]In RC3 galaxy listed as S0.
[h]Bitsakis et al. (2014).

terms of their colours and their spatial extent), while being less strict about the lower luminosity limit (see Fig. 1). These two subcategories are not mutually exclusive, i.e. the same cluster may be present in both categories. Indeed, the selection criteria (described in detail in the section below) for the GCCs are fine-tuned to filter out potentially young SCs in the dynamically young groups with active star formation (e.g. HCG 31) where we detect many young SCs. Thus, we expect to see a small fraction of SCCs being classified as GCCs in such groups (for HCG 31 out of 338 SCCs only 13 of them, or less than 4 per cent, are also GCCs). On the other hand, in a group such as HCG 42, which in our sample is represented by the giant elliptical NGC 3091 and where the majority of the detected sources are expected to be old SCs, we anticipate a majority of SCCs to be also classified as GCCs (out of 356 SCCs for HCG 42, 331 of them, or ∼93 per cent are classified as GCCs). Hence, we use the SCC sample primarily to study the young SC populations and GCCs to study GC populations.

Throughout the paper we use the terms young, intermediate, and old when we talk about SCs. These are general terms without standard definitions in the literature. For this paper, when we talk about young SCs we mean clusters that are younger (according to their location in *BVI* colour space) than 10 Myr. For intermediate clusters, the age range is between a low hundreds of Myr and a few Gyr, and for the old clusters the range is from ∼5 to 14 Gyr. The intervals not covered by our definitions are grey areas, and SCs in those intervals are labelled according to context. For example, if we are talking about intermediate age clusters (750 Myr old), clusters less than 50 Myr old could be referred to as young/younger SCs. For most of the cases, whenever we are using these terms (young, intermediate, old), we are specifying the time intervals within the parentheses following the term.

3.1 Star cluster selection

For the ACS observations, the closest group is HCG 07 at a distance of 56.6 Mpc (from the initial radial velocity measurement by Hickson (1982) modified based on the velocity field model of Mould et al. (2000)), equivalent to a distance modulus of $(m - M)_0 = 33.76$ mag. At this distance, the 0.049-arcsec pixel size of the ACS corresponds to 13.7 pc. The distance to Stephan's Quintet which was observed with the WFC3, is adopted to be 88.6 Mpc (Hickson 1982; Mould et al. 2000), equivalent to $(m - M)_0 = 34.74$ mag. Thus, one 0.04-arcsec pixel on WFC3 corresponds to ∼17.2 pc. With the average SC half-light radius of ∼4 pc (e.g. Larsen 2004; Barmby et al. 2006; Scheepmaker et al. 2007), the majority of the detected clusters in all observations are expected to be unresolved or marginally resolved in the case of the closest groups (e.g. Harris 2009). Therefore, for this catalogue we used point spread function (PSF) fitting as the preferred method of obtaining photometry. In the next section, we give a more detailed explanation for favouring PSF photometry.

For point source detection we used the V_{606} images, as they offer the faintest limiting magnitudes at 50 per cent completeness level among the observations (see Table 5). To detect point sources, we

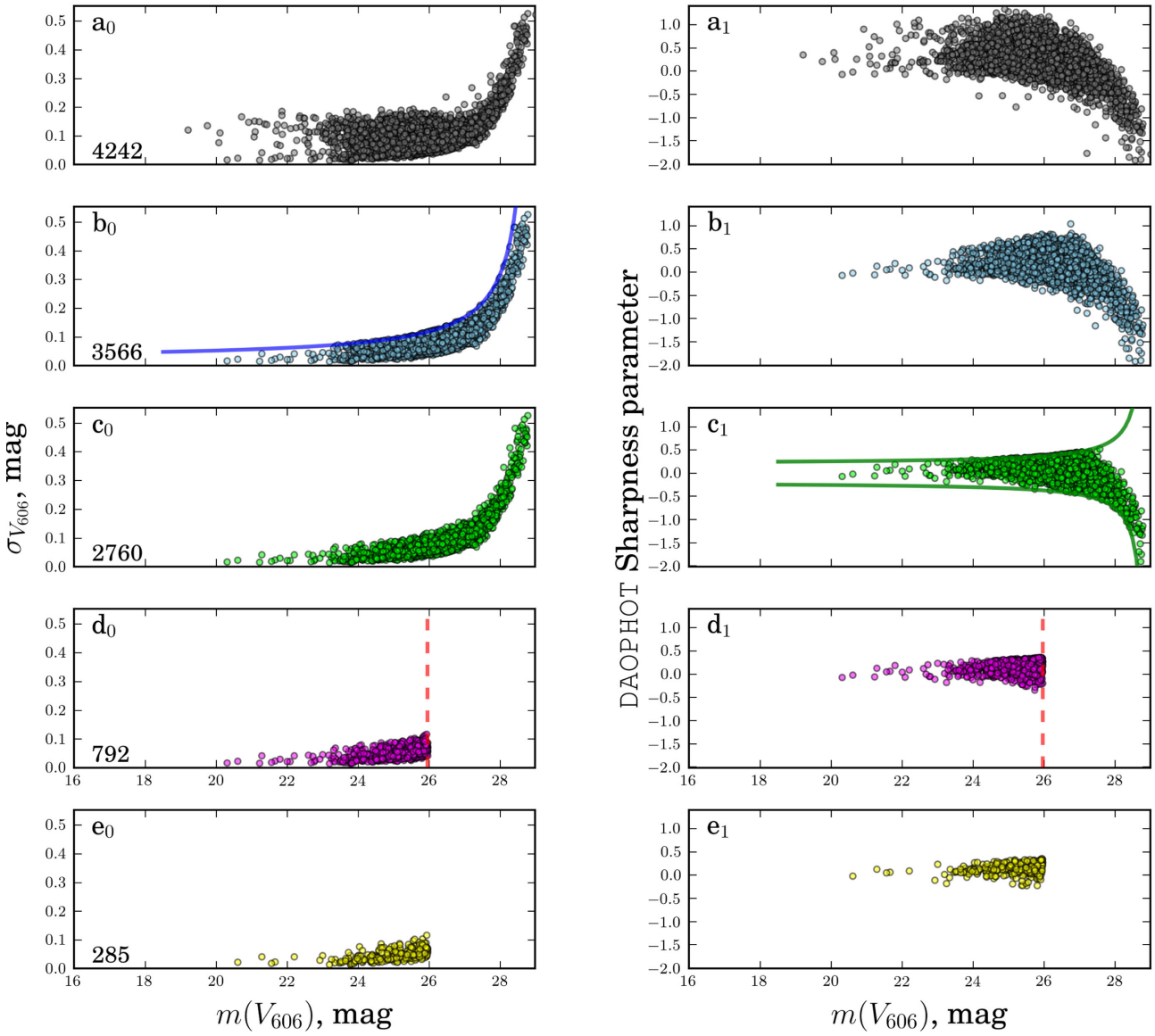

Figure 1. Illustration of the criteria applied to the HCG 07 extended point source catalogue to produce the GCC sample for that group. The rows in this figure show the same point sources being plotted in error, $\sigma_{V_{606}}$, versus V_{606} magnitude (left-hand-side panels with subscript 0) and in DAOPHOT sharpness parameter versus V_{606} magnitude space (right-hand-side panels with subscript 1). The upper row of panels shows the initial point sources. We apply the hyperbolic filter in magnitude error, as observed in panel b_0, and panel b_1 represents the point sources that satisfy that criterion in sharpness parameter space. Panel c_1 shows the hyperbolic filter that was applied in the sharpness parameter space, and c_0 displays point sources in magnitude error space that pass that filtration. We apply a magnitude cut ($M_{V_{606}} < -7.8$) which is illustrated by panels d_0 and d_1. To obtain the final GCC sample for HCG 07, we select only those sources that have colours similar to those of the Milky Way globulars (see Fig. 7, panel a for reference). Resulting objects are presented in panels e_0 and e_1. The number in the lower left corner of the left-hand-side panels indicates the number of point sources that remain after application of each criterion.

run the DAOFIND (Stetson 1987) task in IRAF[2] on median-divided images, obtained by division of the original images by median boxcar-smoothed ones (with a 13×13 pixel smoothing window). The coordinates of point sources detected in V_{606} were transformed into the $B_{435/438}$ and I_{814} coordinate systems. PSF photometry was performed on each image independently, and the results were cross-matched (with matching radius of 1.5 pixels) to yield point sources that were present in all three frames.

PSF models for each filter of each group were constructed from bright, isolated, and unsaturated stars with smooth radial curves of growth. The aperture correction was calculated as an average of the difference between magnitudes obtained from aperture photometry (with a 10 pixel aperture) and PSF magnitudes (calculated at 3 pixels). The aperture corrections between 10 pixels and infinity in the case of ACS observations were taken from Sirianni et al. (2005), and in the case of WFC3 observation were calculated from the enclosed energy curves as the difference between unity and the enclosed energy in the given aperture and wavelength (Whitmore, private communication). The foreground extinctions were obtained

[2] IRAF is distributed by the National Optical Astronomy Observatory, which is operated by the Association of Universities for Research in Astronomy (AURA) under cooperative agreement with the National Science Foundation.

Table 3. Information on number of stars used to create a PSF model, aperture corrections, and foreground extinctions in *BVI* filters for every pointing.

Group	Pointing	# of PSF stars			Foreground extinction			Aperture correction					
								B_{435}		V_{606}		I_{814}	
		B_{435}	V_{606}	I_{814}	B_{435} (mag)	V_{606} (mag)	I_{814} (mag)	$3 \rightarrow 10$ (mag)	$10 \rightarrow \infty$ (mag)	$3 \rightarrow 10$ (mag)	$10 \rightarrow \infty$ (mag)	$3 \rightarrow 10$ (mag)	$10 \rightarrow \infty$ (mag)
HCG 07	1	8	8	6	0.081	0.056	0.036	0.144	0.107	0.209	0.088	0.213	0.087
	2	10	12	12	0.081	0.056	0.036	0.223	0.107	0.139	0.088	0.224	0.087
HCG 31	1	13	13	18	0.210	0.144	0.093	0.161	0.107	0.121	0.088	0.211	0.087
HCG 42	1	24	41	55	0.174	0.119	0.078	0.107	0.107	0.113	0.088	0.030	0.087
HCG 59	1	8	11	9	0.151	0.104	0.066	0.137	0.107	0.162	0.088	0.203	0.087
	2	11	8	16	0.151	0.104	0.066	0.160	0.107	0.174	0.088	0.221	0.087
HCG 92	1	27	14	48	0.32	0.22	0.14	0.207	0.110	0.258	0.103	0.342	0.108

Notes. Foreground extinction coefficients in this table were obtained with Schlegel, Finkbeiner & Davis (1998), published in NED. $3 \rightarrow 10$ aperture corrections were calculated as the mean brightness difference of the stars we used to construct the PSF, between the 3 pixel PSF photometry and brightness measured in a 10 pixel aperture. $10 \rightarrow \infty$ aperture corrections for ACS observations were taken from Sirianni et al. (2005). $10 \rightarrow \infty$ aperture corrections for WFC3 observations were calculated as the difference between unity and the enclosed energy in the given aperture.

from Schlafly & Finkbeiner (2011), published in the NASA/IPAC Extragalactic Database (NED).[3] Table 3 gives overall information on the number of stars used in the PSF constructions, the aperture correction values, and foreground extinctions for different filters and targets.

At this stage, we had an unfiltered point source list for each group, which we refer to as the 'extended sample'.

3.2 PSF photometry justification

Quite often in studies of extragalactic SCs, the question of which type of photometry to use (aperture or PSF) arises. If SCs can be resolved, then, logically, aperture photometry would produce the most accurate results. On the other hand, for unresolved objects PSF photometry is preferred. What about sources that are marginally resolved? Harris (2009) have shown that if a SC is larger than ∼10 per cent of the full width at half-maximum of the stellar PSF then it can be treated as marginally resolved and aperture photometry should be applied. This result is certainly important for studies that look at SC sizes, but what about work that is focusing on the colours (and colour-based properties such as ages) of these SCs.

Colours are differences between the magnitudes in different filters and as such are less dependent on the accuracy of the total magnitude measurements than the relative magnitudes. That is, if measurements are carried out consistently for all of the filters, the magnitude differences between filters (i.e. the colours) should be similar for both PSF and aperture photometry. For our study, most of the CGs are at distances where their SCs may be marginally resolved, except, perhaps HCG 92 (at 88.6 Mpc). However, most of our groups have areas with highly variable backgrounds, and in some cases, albeit rarely, the issue of crowding arises. The above concerns lead us to prefer PSF photometry. Additionally, if a PSF for a given filter is generated and applied correctly, PSF photometry can potentially give more accurate magnitude measurements than aperture photometry, and with much smaller uncertainties.

We have compared the aperture photometry with our PSF photometry and found that the difference between the two are within the accepted error level for this study (<0.17 mag). Moreover, as was mentioned previously, the differences in the photometries becomes even less noticeable in colour indices (<0.09 mag). Thus, we conclude that on average the two photometries produce comparable results, and we prefer PSF photometry for the reasons given above.

[3] http://ned.ipac.caltech.edu/ngi/

3.3 Star cluster candidate selection

To create a catalogue of high-confidence SCCs, we applied to our extended samples the following selection criteria:

(1) *Magnitude cut at* $\boldsymbol{M}_{V_{606}} < -9$ *mag (S1)*
To eliminate the contamination from individual luminous supergiants, which can reach $M_{V_{606}} \simeq -8$ mag, we only considered sources with $M_{V_{606}} < -9$ mag. This roughly corresponds to a cluster mass of a few $\times 10^4\,M_\odot$ at 10 Myr and $\sim 10^6\,M_\odot$ at 10 Gyr (depending on metallicity and distance modulus).

(2) *Photometric error* $\boldsymbol{\sigma} < 0.3$ *mag in all three filters (S2)*
To maintain photometric quality of magnitudes and colours, all point sources that had photometric errors larger than 0.3 mag in any of the $B_{435/438}$, V_{606}, or I_{814} filters were discarded.

(3) *Sharpness between −2 and 2 in all bands (S3)*
To further minimize contamination from cosmic rays and background galaxies, we applied a sharpness filter which, essentially, is a constraint on the intrinsic angular size of the detected objects. Sharpness is measured as the difference between the square of the width of the object and the square of the width of the PSF, and for our purposes should be between −2 and 2: large positive values of sharpness are indicative of blended sources and partially resolved galaxies, whereas large negative numbers are flags for cosmic rays and blemishes. For a well-matched width the sharpness is zero.

(4) $\boldsymbol{\chi} < 3$ *in the* I_{814} *band (S4)*
The DAOPHOT goodness of fit factor χ from PSF fitting in the I_{814} band should be less than 3. The use of I_{814} band for the χ parameter is twofold: (a) the PSF model is typically best determined in that band because we have the most PSF stars; and (b) no contamination from nebular emission lines (e.g. Hα) is expected (nebular emission around a young SC may cause them to be marginally resolved in the V_{606}-band images).

(5) *Colour cuts (S5)*
In order to minimize the contamination from foreground Galactic stars, we applied colour cuts, where all sources that had colours $B_{435/438} - V_{606} > 1.5$ mag or $V_{606} - I_{814} > 1.0$ mag were discarded. As can be seen in fig. 8 of Trancho et al. (2012), applying these colour cuts removes the majority of spectroscopically confirmed contaminants.

Table 4. Percentage remaining of the initial sources after applying particular criteria.

Group	Number of initial sources	S1 (per cent)	S2 (per cent)	S3 (per cent)	S4 (per cent)	S5 (per cent)	SCC (per cent)	G1 (per cent)	G2 (per cent)	G3 (per cent)	G4 (per cent)	GCC (per cent)	N_{common}
HCG 07	4243	11.6	91.3	100.0	92.3	88.3	6.9	84.0	66.1	40.6	28.2	6.7	86
HCG 31	2670	25.5	93.7	99.9	84.1	88.8	12.7	64.4	44.7	58.6	22.3	2.9	13
HCG 42	2262	22.1	94.7	99.7	94.2	82.2	15.7	92.1	85.2	58.5	67.8	39.7	331
HCG 59	3445	12.9	76.3	99.9	93.5	84.7	7.5	78.8	79.6	41.1	39.1	10.9	121
HCG 92	5493	52.9	94.5	99.3	82.9	78.7	29.4	92.4	81.4	92.6	23.5	17.2	341

Notes. Criteria S1–S5 are for SCs, criteria G1–G4 are for GCs; S1 – magnitude cut at $M_{V_{606}} < -9$ mag; S2 – photometric error less than 0.3 mag in all three frames; S3 – sharpness between −2 and 2 in all bands; S4 – χ in I filter less than 3; S5 – colour cuts; G1 – hyperbolic filter in the magnitude errors; G2 – hyperbolic filter in the sharpness; G3 – magnitude cut at $M_{V_{606}} < -7.8$ mag; G4 – colours similar to those of the dereddened Milky Way GCs. SCC and GCC columns show the resulting percentage of high-confidence star and GCCs, respectively. N_{common} column shows the number of clusters that appear in both SCC and GCC catalogues.

3.4 GCC selection

In a similar manner, we created a catalogue of GCCs, with the following (generally stricter) criteria (based on Rejkuba et al. 2005):

(1) *Hyperbolic filters in photometric error (G1)*
The hyperbolic filter in the photometric error was defined in such a manner as to retain ∼97 per cent of all recovered artificial sources (these are the sources that were used in determining the completeness level, see Section 3.5). The application effect of this filter on detected sources can be observed in Fig. 1, panels b_0 and b_1.

(2) *Hyperbolic filters in* DAOPHOT *sharpness parameter (G2)*
We defined the hyperbolic filter in the V_{606} DAOPHOT sharpness parameter in the same manner as the photometric error filter. That is, the sharpness filter is tuned so that it retains ∼97 per cent of all recovered artificial sources. However, there is a possibility that for the closest groups (e.g. HCG 07, HCG 42) some of the GCCs might be marginally resolved. In these cases, we relax the upper envelope of the sharpness filter to make sure that we do not discard larger GCCs. The example of the application and effect of the sharpness filter on detected sources can be seen in Fig. 1, panels c_0 and c_1.

(3) *Magnitude cut at* $\boldsymbol{M}_{V_{606}} < -7.8$ *mag (G3)*
Because contamination from supergiants is less of a problem for objects with GC-like colours, we relaxed our luminosity cut to $M_{V_{606}} < -7.8$ mag to get closer to the expected peak of the GC luminosity function (GCLF) $M_V \sim -7.4$ (e.g. Ashman & Zepf 1998; Harris 2001). The −7.8 mag cut-off roughly corresponds to a GC mass of $\sim 5 \times 10^5\,M_\odot$ (depending on metallicity and distance modulus). The effect of application of this filter is shown in Fig. 1, panels d_0 and d_1.

(4) *Milky Way Globular Cluster selection parallelogram (G4)*
We use dereddened GCs from the updated Harris (1996) Milky Way Globular Cluster catalogue to derive a selection parallelogram in $B - V$ versus $V - I$ colour space. We convert the vertices of the parallelogram from Johnson's B, V, I magnitudes to B_{435}, V_{606}, I_{814} magnitudes via transformations derived from Sirianni et al. (2005). We keep all sources that would fall into the selection parallelogram in the $B_{435} - V_{606}$ versus $V_{606} - I_{814}$ colour space or that would overlap the selection region with their 1σ error bars. HCG 92 was observed with WFC3 and there is (to our knowledge) currently no equivalent to the Sirianni et al. (2005) calibration paper for this instrument. Therefore, we apply the same selection box for GCs to these data as for the ACS data. Given the similarities between these two instruments and their filter sets, we would not expect a significant change in the number of GCCs as the result of that action.

Table 4 specifies what fraction (in percent) of the initial number of point sources (rightmost column) remains after applying each criterion individually. For example, after applying the S1 criterion (absolute magnitude cut) on 4243 sources detected in HCG 07 only 11.6 per cent (or 493 sources) of the original sample remains, whereas after applying the S2 criterion (photometric error < 0.3 mag in all three filters) on the initial list of 4243 sources, 91.3 per cent of the extended sample (or 3874 sources) remain, and so on.

3.5 Completeness levels

To determine completeness of our catalogue, we carried out the following routine for each group in our sample. For groups HCG 07, HCG 42, HCG 31 and HCG 59 we used ADDSTAR to add 3000 artificial stars to the images (over the entire field, including the galaxies) in the apparent magnitude range 24–28 mag, i.e. absolute magnitudes ranging between −9.99 and −5.76 mag (taking into consideration that these groups are located in the range of distances from 56.6 and 62.8 Mpc). For HCG 92 we used ADDSTAR to add 5000 artificial stars to the image as the image covers a larger field of view. The apparent magnitude range of artificial stars was the same, i.e. 24–28 mag, which translates into absolute magnitudes range between −10.74 and −6.74 mag, given that the distance modulus for HCG 92 is 34.74 mag. After artificial stars were added to the images, we applied the same algorithm for point source detection to determine the recovery rates. The average limiting magnitudes for the 50 and 90 per cent recovery rates for each group are presented in Table 5. As can be seen, we operate at the slightly higher than 90 per cent completeness level (in V_{606} filter) for GCCs and at even higher completeness level for the SCCs, except for HCG 92 which is the most distant group in our sample. In that case we are at $\gtrsim$50 per cent and ∼90 per cent completeness level for the GCCs and SCCs, respectively. We point out that the method described gives the values for the average completeness level over the entire image. Because of the random distribution of artificial sources and because galaxies (with elevated surface brightness) typically take up a smaller fraction of the field of view, our actual completeness levels will generally be lower as SCs tend to be found in galaxies (with HCG 92 as a notable exception).

The level of completeness becomes especially important when we are dealing with the specific frequencies and metallicity distributions for GCCs. The $B - V$ colour for GCCs is, on average, about 1 although our selection parallelogram (the G4 criterion, Section 3.4) goes down to $B - V = 1.38$. As an example, consider a hypothetical GCC source in HCG 42. If this source has $m_V = 26$ mag (just above the 90 per cent completeness level in the V filter; Table 5), its magnitude in B, according to our G4 criterion, will be between

Table 5. Completeness levels for our HCG sample.

Group	B_{435}		V_{606}		I_{814}		Distance	GCC cut-off	SCC cut-off
	50 per cent	90 per cent	50 per cent	90 per cent	50 per cent	90 per cent	modulus	$M_{V_{606}} < -7.8$ mag	$M_{V_{606}} < -9$ mag
HCG 07	27.4	26.7	27.5	26.3	27.1	26.4	33.76	25.96	24.76
HCG 31	27.3	26.7	27.4	26.4	27.2	26.5	33.68	25.88	24.68
HCG 42	27.2	26.2	27.2	26.1	27.1	26.0	33.86	26.06	24.86
HCG 59	27.2	26.6	27.2	26.5	27.1	26.5	33.99	26.19	24.99
HCG 92	26.9*	25.9*	27.1	26.0	27.0	25.9	34.74	26.94	25.74

Notes. The values for distance moduli were taken from NED with the following cosmology parameters: $H_0 = 73.0$ Mpc km s^{-1}, $\Omega_{\rm matter} = 0.27$, and $\Omega_{\rm vacuum} = 0.73$.
*For HCG 92 B filter is B_{438} of WCF3 camera.

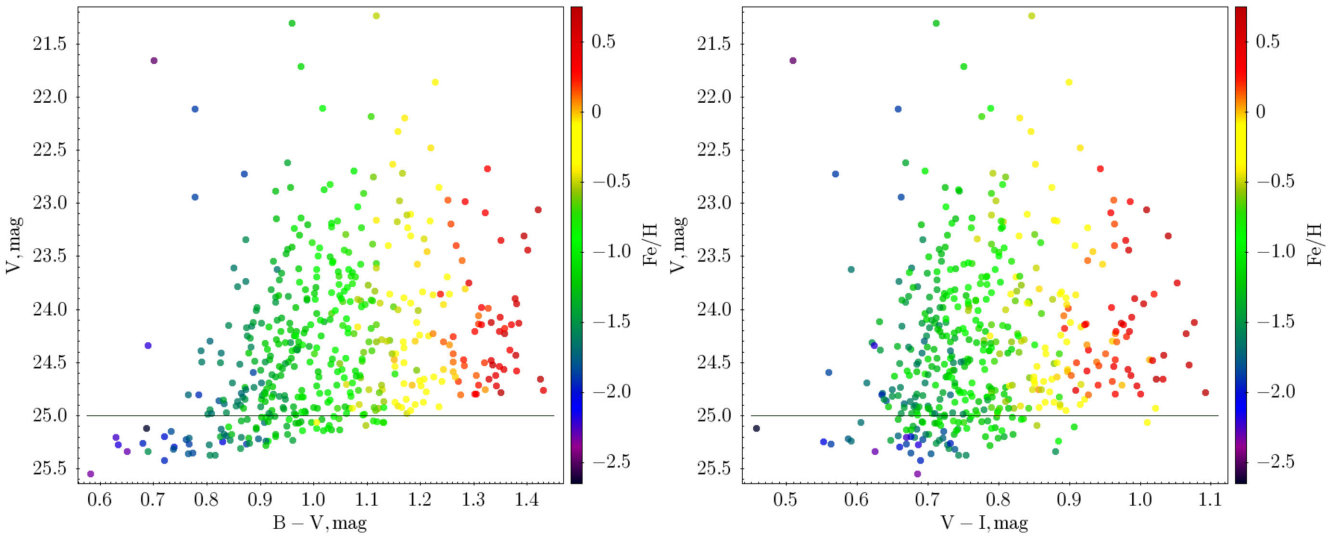

Figure 2. $B - V$ and $V - I$ colour–magnitude diagrams for HCG 42. The displayed sources are GCCs at or above 90 per cent completeness level in all three filters. The sources themselves are colour coded according to their metallicities (see Section 3.7), represented with colour bars on the right-hand side of each plot. As can be seen from the plots, even at the 90 per cent completeness level we are still missing some of the metal enriched GCCs. To minimize this effect, we are making a magnitude cut at $V = 25$ mag for this group, and at $V = 25.5$ mag for HCG 07, HCG 31, and HCG 59. Thus, for obtaining values of the expected total number of GCs in a galaxy, $N_{\rm total}$, the value of specific frequency, S_N, or for the analysis of the metallicity distribution of GCCs we will be using a subcatalogue with aforementioned magnitude cut.

26.68 and 27.38. However, the 90 per cent completeness level in B is 26.2 mag. Thus, if we force our sources to have 90 per cent completeness level only in the V filter, we will be missing some of the red sources at the faint end. Moreover, even forcing 90 per cent completeness in the limiting filter (in our case it is B filter), we are still risking missing some objects (Fig. 2). So, for the calculation of the total number of clusters in the GC system of a host galaxy, the GC specific frequency, and the metallicity distributions, we will be using a portion of our catalogue, in which all sources are at or above 90 per cent completeness level in all three filters and which also minimizes the loss of the faint metal rich GCCs. For our sample of HCGs, that corresponds to V-filter magnitude cut-offs at 25.0 mag for HCG 42, and 25.5 mag for HCG 07, HCG 31, and HCG 59. The only exception is HCG 92, the farthest group in our sample. For this group we went down to 50 per cent completeness level, to maximize the number of GCCs to strengthen the statistical conclusions validity. Unfortunately, even at that completeness level, we are still sampling only about 10 per cent of the GCLF making the derived values of the total number in the GC populations ($N_{\rm total}$) and specific frequencies (S_N) of HCG 92 galaxies highly uncertain (∼factor of 5). Although we forego determining $N_{\rm total}$ and S_N for HCG 92 (for aforementioned reasons), we are still attempting a GCC population analysis, based on a 'face value' GCC catalogue containing sources that are at or above the 50 per cent completeness level with a cut-off at $V = 25.5$ mag (to minimize the loss of the faint metal rich GCCs).

3.6 Physical extent of the SCC and GCC systems

For each group, we present an image with regions that define the expected extent of the SC and GC systems for each galaxy in that group. We define the extent of the SC systems as a brightness contour of $\sim 1.25\sigma$ above the background level in the V_{606} image to trace the stellar light in each galaxy. The value of 1.25σ was identified after experimenting with different values to both cover the optical extent of the galaxies and include the apparent SC populations. We successfully applied this criterion in our previous studies, and we enclose areas large enough to include sources that are likely associated with the host galaxies. To define the expected extent for the GC systems (which populate much fainter galaxy haloes), we initially use the formula outlined in Rhode et al. (2007):

$$y = [\,(45.7 \pm 9.5)\,x^2\,] - [\,(985 \pm 217)\,x\,] + (5320 \pm 1240), \quad (1)$$

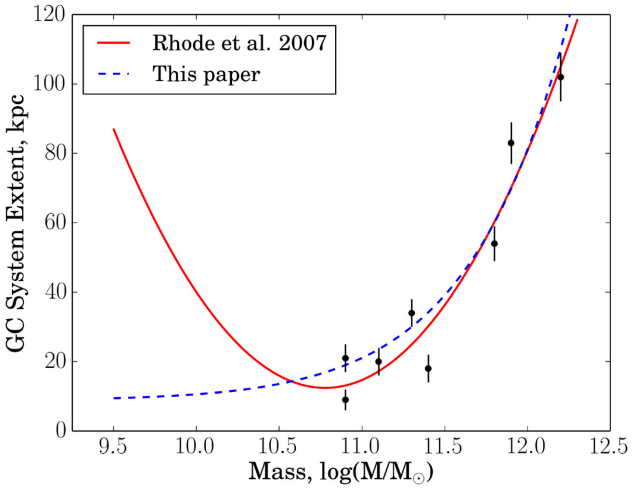

Figure 3. The relation between the expected extent of a GC system from Rhode et al. (2007, solid line) and the modified version used in this paper (dashed line). The modified relation was meant to be used only on the mass range presented in this plot (i.e. from 10^9 to $\sim 10^{12.5}$ $M_\odot$). The black dots are from the sample of Rhode et al. (2007), which consists of the radial extent of the GC system and the galaxy mass in solar masses for nine elliptical, S0, and spiral galaxies from their wide-field GC system survey.

where x is the mass of a host galaxy in $\log(M/M_\odot)$ and y is the expected radial extent of a system in kpc. However, given the quadratic nature of the above equation and the low mass of some galaxies in our sample, we needed to modify that expression to get more realistic numbers for the lower range of stellar masses. We made an assumption that for a small galaxy with a mass of $10^9 M_\odot$, the expected radial extent of the GC system would be 9 kpc. This assumption is supported by observed GCC distributions in galaxies in our HCG sample. Combining that with data of the GC systems extent from Rhode et al. (2007) and fitting a power-law function, we obtain the following relation:

$$y = 8.85 + (6.6 \times 10^{-21})\, x^{20.42}, \quad (2)$$

with x and y defined as above. This relation is valid for the range of log(mass) values from 9 to 12.5 $M_\odot$. The result (dashed line) can be seen in Fig. 3.

3.7 Photometric estimates of metallicity

We use the Sirianni et al. (2005) synthetic transformations to convert $(B - I)$ colours for GCs to the Johnson photometric system $(B - I)_0$ colours. We estimate the GC metallicities using the $(B - I)_0$ to [Fe/H] transformation from Harris et al. (2006):

$$(B - I)_0 = 2.158 + 0.375[\mathrm{Fe/H}]. \quad (3)$$

For the GC population of our sample galaxies with a sufficient number of clusters (we use populations with 40 or more GCs), we plot the $(B - I)_0$ colour distribution and measure the specific frequency. We also plot $(B - I)_0$ colour distributions of GCs for each galaxy group in our sample. We use the GMM (Gaussian Mixture Modelling) code of Muratov & Gnedin (2010) to probe the bimodality and to determine the peaks and dispersions of these distributions. Because mixture modelling codes are generally sensitive to extended tails we use GMM on the distribution between $-2.5 <$ [Fe/H] < 1.0. The GMM results are recorded in Table 6 similarly to table 2 of Blakeslee et al. (2012), where one can find a detailed guide to interpreting the GMM results. The plots of the metallicity distributions for groups and galaxies from Table 6 are presented in Figs 7, 9, 11, 13 and 15, and described on a group-by-group basis in Section 4 below.

3.8 Empirical estimate of GC system population

In a recent work, Harris, Harris & Alessi (2013) have determined an empirical predictor of the total number of GCs for galaxies of

Table 6. GMM results of probing modality of metallicity distributions.(p italic in p1 p2)

Group/Galaxy (1)	N (2)	Kurt (3)	p-val (4)	p1 (5)	p2 (6)	D (7)	Frac(2) (8)	Bimodal (9)
HCG 07	165	−0.748	0.115	-1.21 ± 0.23	-0.08 ± 0.26	2.46 ± 0.32	0.21 ± 0.19	No
HCG 07BD	83	−0.576	0.442	-0.86 ± 0.23	0.31 ± 0.27	2.73 ± 0.57	0.07 ± 0.18	No
HCG 42	400	−0.598	0.001	-1.05 ± 0.07	0.15 ± 0.14	3.14 ± 0.33	0.25 ± 0.08	Yes
HCG 42A	393	−0.611	0.001	-1.04 ± 0.07	0.16 ± 0.15	3.14 ± 0.35	0.26 ± 0.08	Yes
HCG 59	198	−0.475	0.592	-1.20 ± 0.46	-0.37 ± 0.33	1.69 ± 0.63	0.20 ± 0.33	No
HCG 59B	112	−0.306	0.803	-1.05 ± 0.36	-0.43 ± 0.28	1.36 ± 0.80	0.38 ± 0.29	No
HCG 92	290	−0.575	0.004	-0.79 ± 0.62	0.63 ± 0.53	2.65 ± 0.39	0.09 ± 0.36	Yes
HCG 92BD	67	−0.541	0.766	-0.46 ± 0.20	0.68 ± 0.32	2.76 ± 0.76	0.07 ± 0.19	No
HCG 92C	46	−0.814	0.010	-0.79 ± 0.34	0.59 ± 0.34	3.24 ± 0.61	0.18 ± 0.22	Yes?
HCG 92E	52	−0.608	0.738	-0.93 ± 0.28	0.09 ± 0.29	2.36 ± 0.67	0.29 ± 0.20	No

Notes. Columns list: (1) group, galaxy or region for which modality is being determined; (2) number of analysed GCs in given distribution; (3) kurtosis of the input distribution; (4) an indicator of the significance of a bimodal Gaussian over a unimodal Gaussian distribution (lower p-values are more significant); (5) mean of the first peak of the proposed bimodal Gaussian distribution; (6) mean of the second peak of the proposed bimodal Gaussian distribution; (7) separation of the peaks; (8) the fraction of GCCs that was assigned to the second peak of bimodal Gaussian distribution; (9) our expectation on bimodality of the given distribution based on the evidences displayed in this table. For the purpose of statistical significance only galaxies/regions with over 40 GCCs were checked for bimodality. The GCCs that were used for this purpose were all at or above 90 per cent completeness level (except for HCG 92, where sources were at or above 50 per cent completeness level). To minimize the loss of the faint metal enriched GCCs, we further apply a $V = 25.5$ mag cut ($V = 25.0$ mag for HCG 42). All these manipulations reduce the GCC numbers available for analysis, but at the same time, bring our completeness to 95 per cent level for HCG 07, HCG 31, HCG 42, and HCG 59.

Table 7. General properties of GCC systems in galaxies in our sample.

Galaxy (1)	N_{GCC} (2)	N_{contam} (3)	N_{total} (4)	S_N (5)
HCG 07A	62 ± 14	2 ± 1	226 ± 73	0.7 ± 0.2
HCG 07BD	155 ± 22	2 ± 1	580 ± 150	2.5 ± 0.8
HCG 07C	38 ± 6	2 ± 1	140 ± 39	0.6 ± 0.2
HCG 31AC	19 ± 5	1 ± 1	67 ± 23	0.6 ± 0.2
HCG 31B	10 ± 3	1 ± 1	35 ± 14	1.0 ± 0.4
HCG 31G	8 ± 3	1 ± 1	28 ± 13	0.7 ± 0.3
HCG 42A	465 ± 26	4 ± 2	3420 ± 1710	2.6 ± 1.3
HCG 59A	18 ± 5*	1 ± 1**	86 ± 33	0.7 ± 0.3
HCG 59B	106 ± 11	1 ± 1**	507 ± 150	8.7 ± 2.6
HCG 59C	≤ 2	1 ± 1**	<10	<0.1
HCG 92BD	10 ± 4	5 ± 2	–	–
HCG 92C	1 ± 3	4 ± 2	–	–
HCG 92E	5 ± 3	2 ± 1	–	–

Notes. Columns list: (1) galaxy id; (2) number of detected GCCs in the system's extent. The GCCs presented here are all at or above the 90 per cent completeness level in all three filters. Additionally, *V*-filter magnitude cut-offs were applied at 24.5 mag for HCG 92, 25.0 mag for HCG 42, and 25.5 mag for HCG 07, HCG 31, and HCG 59. The reasons for doing so are explained in Section 3.5. If the full system extent is not visible, detected numbers of GCCs are scaled to estimate the numbers of the full system extent. Foreground contamination is taken into account, i.e. subtracted from the number of detected GCCs; (3) estimated number of contamination sources from Besançon Milky Way stellar population model (Robin et al. 2003) in the direction of the group up to the distance of 100 kpc, with colours similar to MW GC colours and in the visible area of GC system extent; (4) estimated total number of GC population based on GCLF; (5) specific frequency.

*Because GCC extent of 59A overlap sources from 59D (which are, most likely, reddened young SCs), the predicted number of GCCs for 59A galaxy was obtained by subtraction of 59D sources from all detected sources in that region.

**For HCG 59, the background contamination is much higher (4 ± 2), due to the close proximity of the Sagittarius dwarf galaxy (Konstantopoulos et al. 2012).

all luminosities as a function of effective radius (R_e) and velocity dispersion (σ_e), given by equation

$$N_{GC} = (600 \pm 35) \left[\left(\frac{R_e}{10\,\mathrm{kpc}} \right) \left(\frac{\sigma_e}{100\,\mathrm{km\,s^{-1}}} \right) \right]^{1.29 \pm 0.03}. \quad (4)$$

For those galaxies in our sample for which we were able to find the values of R_e and σ_e in the literature (HCG 42A and HCG 59B), we calculate the predicted numbers of GCs and compare them to our estimates (Table 7) based on the observed GCLF in each galaxy.

4 RESULTS AND DISCUSSION

Below, we present a short overview of the SC populations in our sample of HCGs. Analyses of the data presented in this catalogue for individual groups have been published in a number of publications (e.g. Gallagher et al. 2010; Konstantopoulos et al. 2013). However, most of these analyses were on a case-by-case basis. In this publication, we aim for a systematic approach by applying the same criteria to the catalogue selection as whole. Because of this, there will be some differences between already published results and the numbers obtained in this paper. For example, the total number of GCCs may differ because we apply a different magnitude cut-off or use a slightly modified distance modulus. Throughout the

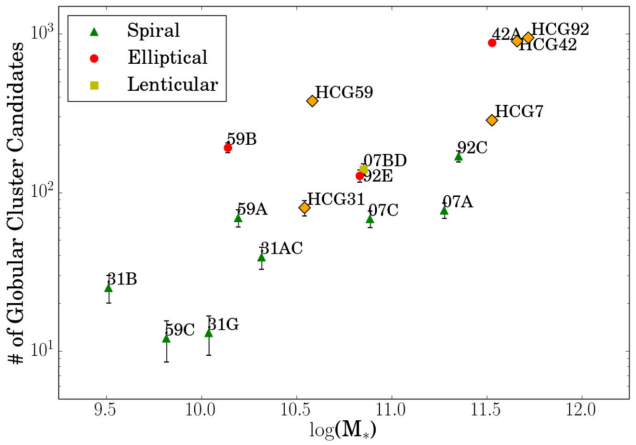

Figure 4. Plot of the number of GCCs ($M_{V_{606}} < -7.8$) in a galaxy versus its stellar mass. Large diamonds represent HCGs, where the total number of GCs in each group is the summation of GCs of its individual galaxies. Similarly, the mass of a group is the summation of the stellar masses of all galaxies in that group from Desjardins et al. (2014). The masses were determined by SED fitting and the reported errors (Desjardins, private communication) are not derived from the photometric uncertainties but rather from the fitting, and are very small (not visible behind the symbols). From this plot we can see that 59B has a very large GC population, on par with the total numbers for some individual groups. The region 07BD is presented here as a lenticular galaxy because the dominant galaxy B – expected to have the most GCCs of the two – is lenticular.

paper, we carefully outline all of our steps so the reader can follow them and, if desired, modify them to apply their own criteria.

Furthermore, we examine the SC populations of CGs through the prism of the formation history and evolution of those groups. As mentioned previously, Konstantopoulos et al. (2010) outlined a proposed evolutionary sequence of CGs with respect to the amount and spatial distribution of cold gas in these groups. In brief, using the ratio of gas mass to the dynamical mass, the groups are divided into three types: I, II, and III for gas-rich, intermediate, and gas-poor groups. Moreover, these groups are further split into two parallel sequences, depending on the location of gas inside a group. Sequence A is for groups with gas contained in galaxies, and Sequence B is for groups with gas being dispersed throughout the IGM. Our sample represents all three types of groups in terms of gas content, and so we can trace differences between the group types through the lens of their SC populations.

To check the general properties of galaxies in our sample we plot two figures. First, we plot the number of detected GCCs in galaxies as a function of stellar masses of those galaxies, Fig. 4. On average, the numbers of GCCs in a host galaxy are proportional to the stellar mass of that galaxy. However, galaxy 59B, and as the result the whole HCG 59, appears to have an excess of GCs given its stellar mass. This is discussed in Section 4.4 in more detail.

The second plot represents the number of 'blue' SCs (young SCs with ages $\lesssim$10 Myr) in each galaxy as a function of SFR of the host galaxies; Fig. 5. The young SCs were selected by applying the colour cut of $V - I < 0.1$. This generous colour cut enables us to keep the maximum number of young clusters, even those that may have significant reddening, avoiding both the evolutionary track loop around ages of 10 and 100 Myr and the old GC region (see Fig. 6 for reference). The numbers of young SCs behave in a predictable manner as well: the galaxies with higher SFR have a larger number of young SCs. Notably, the large

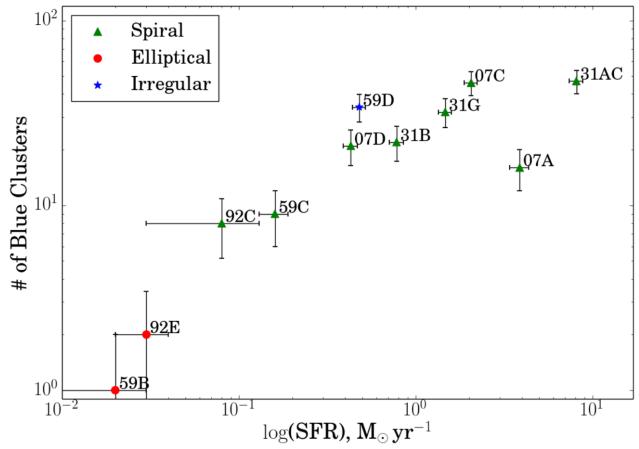

Figure 5. Plot of the number of 'blue' clusters (with colour $V-I<0.1$) in a galaxy versus its SFR. On average, the elliptical galaxies have low SFR with correspondingly low number of 'blue' clusters; spirals have higher number of young clusters and higher SFRs. The relatively high number of young clusters and relatively low SFRs of galaxies 92C and 59C are consistent with a recent end to a star formation phase in these galaxies. However, the young clusters are still numerous and bright enough to be detected. Also, as was noted earlier, galaxies in HCG 07 exhibit elevated SFR, and correspondingly large numbers of young blue clusters, without visible signs of interactions. 59B has only one, 92E has two, and 07B has none of the blue clusters. This is expected given that these are elliptical/lenticular galaxies. The region 31AC is marked as a spiral because the larger of the two interacting galaxies, galaxy A, is classified as spiral.

irregular 59d has a very high number of young SCs given its mass and SFR.

In the subsections below, we discuss the star and GC populations of each group individually.

4.1 HCG 07

4.1.1 Star cluster candidates

This group is classified as a Type II group in the evolutionary sequence, with an intermediate amount of gas contained within the individual galaxies. As first presented in Konstantopoulos et al. (2010), although we do not observe strong signs of interactions between the galaxies in this group, the large number of young SCs indicates that SFRs are at an elevated level (see Fig. 5). From the distribution of clusters within the colour–colour diagrams compared to the simple stellar population models (SSP) of Marigo et al. (2008), galaxies A, C, and D appear to have the youngest SCCs, while B has a more mature population. Most of the youngest SCCs are located down and to the right of the dashed evolutionary track of nebular emission for <10 Myr clusters along the direction of the reddening vector, consistent with the hypothesis that these clusters have $A_V = 1$ to 3 mag. Similarly, Whitmore & Zhang (2002) found that the median extinction value for optically selected very young clusters ($\lesssim$4 Myr) in the Antennae galaxies is 2.6 mag. Moreover, from the distribution of SCCs it would appear that the star formation in galaxy C has a more extended history, whereas galaxies A and D exhibit an onset of more recent star formation (Fig. 6), as shown by lower cluster densities between the ages of 100 Myr and 1 Gyr.

4.1.2 Globular cluster candidates

The colour–colour plots of the GCC population for galaxies in HCG 07 are presented in Fig. 7 and their properties are presented in Table 7. Because galaxies A, C, and D are spiral galaxies (with C and D being face-on galaxies), the number of GCCs in them should be taken with caution. The GCCs located in the central regions and spiral arms may be contaminated by reddened young SCs. For the GCCs of galaxies B and D, we considered the pair as a single object because of the difficulty of distinguishing cluster ownership given the overlap of the expected extent of the GC systems in these galaxies. As derived from the $B-I$ colour, the average metallicities of the GCs in galaxy A (spiral) and the BD (B is lenticular, D is spiral) system are below Solar metallicity and comparable to metallicities of galaxies of comparable luminosity (e.g. Barmby et al. 2000; Kundu & Whitmore 2001; Goudfrooij et al. 2003; Chandar, Whitmore & Lee 2004; Peng et al. 2006). Galaxy A has 43 ± 7 observed GCCs with $V < 25.5$ mag. Compensating for the missing portion of GC system extent, and assuming a circular symmetry, we estimate the total number of observed GCCs as 62 ± 14 (taking in consideration the foreground sources, Table 7). At the given $V = 25.5$ mag cut-off, assuming the GCLF turnover at -7.4 ± 0.2 mag and width $\sigma = 1.2 \pm 0.2$ mag, we sample 28 ± 6 per cent of the GCLF. Taking our completeness fraction as 0.95 ± 0.05, we conclude that for galaxy A ($M_V = -21.31$ mag) the total number of GCCs in the system is $N_{\rm total} = 226 \pm 73$ and specific frequency is $S_N = 0.7 \pm 0.2$. Applying the same approach to other galaxies in the group we find that for the BD region ($M_V = -20.9$ mag for B, $M_V = -19.7$ mag for D) $N_{\rm total} = 580 \pm 150$ and $S_N = 2.5 \pm 0.8$, for C ($M_V = -20.85$) $N_{\rm total} = 140 \pm 39$ and $S_N = 0.6 \pm 0.2$. We note that because galaxies A and C are spiral (A is highly inclined and C is a face-on), a significant number of objects with GC-like colours could, potentially, be reddened young SCs.

4.2 HCG 31

4.2.1 Star cluster candidates

This group – classified as Type I with a cold gas-rich IGM – consists of a number of small galaxies apparently coming together for the first time. The colour–colour plot of all detected SCCs, including those in the IGM, paints a picture of a group that is actively forming stars for the last tens of Myr (panel a of Fig. 8). Simultaneous interactions (e.g. galaxies AC and B) have triggered a very high SFR of 8.11 $M_\odot$ yr^{-1} (Tzanavaris et al. 2010), as shown by the large number of very young SCCs on the colour–colour plots. Virtually all of the SCCs in regions E and F (24 SCCs combined) are younger than 10 Myr. These regions are tidal features connecting spiral galaxy G, interacting pair AC and B, placing a time constraint on the interaction between those galaxies. There is a high concentration of SCCs around the region where the evolutionary track makes a backward loop, essentially making it impossible in this colour-space to distinguish between SCs of 10–100 Myr old (panels c and d of Fig. 8). However, given the low density of SCs older than 300 Myr ($\log(t) \sim 8.5$ yr) and the large number of young SCs ($\lesssim$10 Myr), we consider it likely that most of the SCs in the vicinity of evolutionary track loop are closer to being a few tens of Myr old rather than 100 Myr.

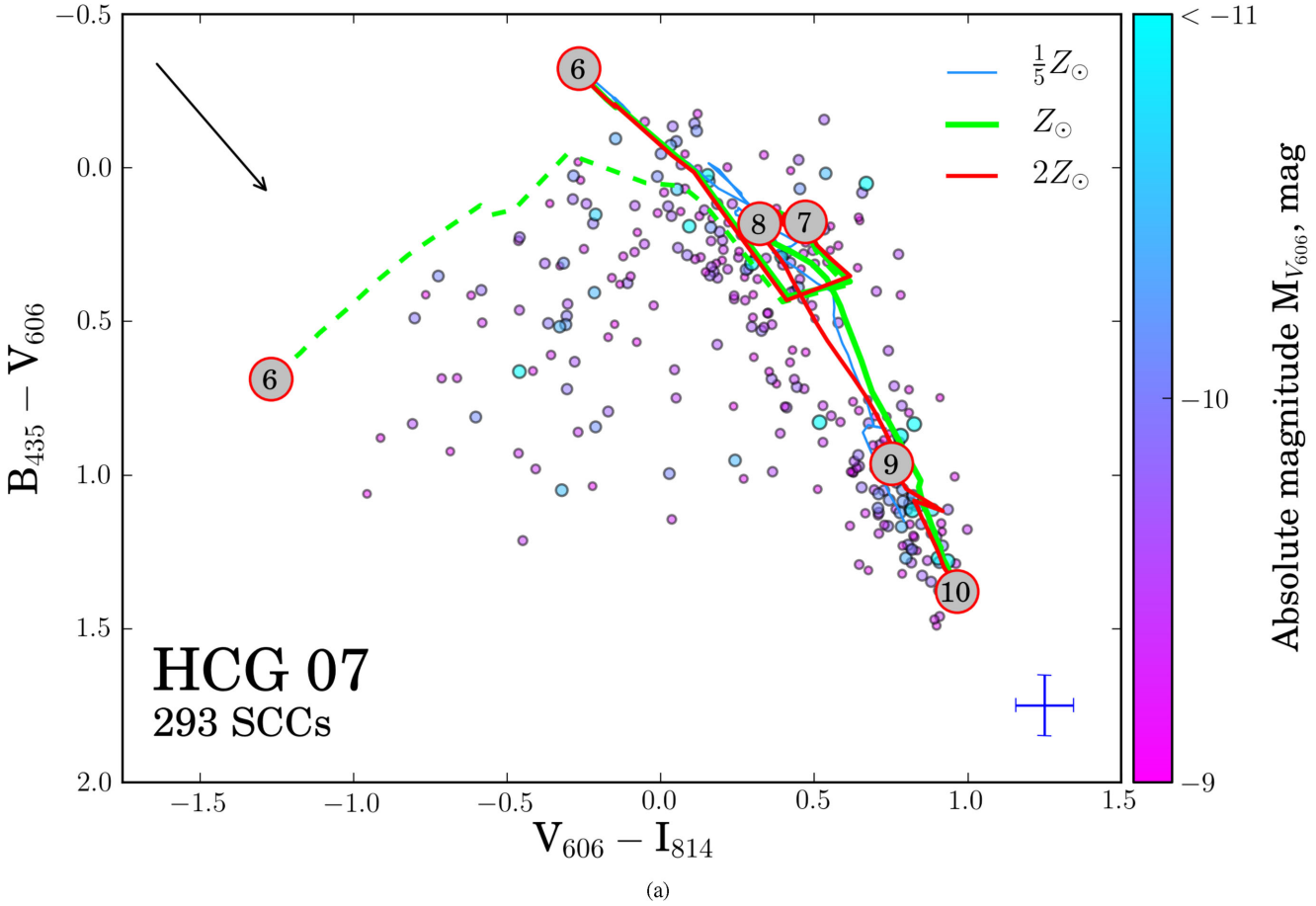

Figure 6. Colour–colour plots of all the SCCs in HCG 07 (a), including clusters located in the IGM. The thin solid line, solid line, and dashed line trace the evolution of SSP models of [0.2, 1.0, 2.0] $Z_\odot$ (Marigo et al. 2008). The thin dashed line to the left of the main evolutionary track represents a track that incorporates a model of nebular emission (Starburst99; Leitherer et al. 1999), common for young SCs (e.g. Vacca & Conti 1992; Conti et al. 1996). The numbers on the track denote age represented in log (age/yr). In the upper left corner one can find a reddening vector with length equivalent to $V_{606} = 1$ mag. The number of SCCs detected in this group is marked in the lower left corner. A typical photometric error bar, based on the median errors, is located in the lower right corner. A colour bar that represents the absolute magnitude of SCCs is given on the right. For ease of reading the plot, the sizes of SCCs in the plot are linearly proportional to their magnitude: the larger the dot, the brighter the SC. All SCCs on this and following plots have absolute magnitude ≤ -9 mag. Panels (b) and (c) are inverted V_{606} images which show the SC system extent of each galaxy as defined by a brightness contour in V_{606} of $\sim 1.25\sigma$ above the background level. Here and in subsequent plots, a compass indicates north (with an arrowhead) and east (without the arrowhead). Panels (d)–(g) are *BVI* colour–colour plots for individual galaxies and regions in the group. The large spiral HCG 7C hosts the greatest number of young clusters, while the quiescent elliptical HCG 7B has only globular clusters.

4.2.2 Globular cluster candidates

The GC population of HCG 31 as expected is rather small, with only 77 sources with colours similar to the Milky Way's GCs (Fig. 9). Most of the clusters are situated within the boundaries of the major galaxies AC, B, and G, and, in all likelihood, are reddened young SCs (especially for galaxies B and G). Additionally, we do not expect a large GC population in this group as the galaxies are not massive enough to host a significant number of GCs with masses (and hence luminosities) large enough to be detectable at such distances. Furthermore, we observe a lack of old (>1 Gyr) SCs in the colour–colour plot for SCCs of HCG 31 (panel a of Fig. 8).

Determining the total number of GCCs and GC specific frequencies in the galaxies of HCG 31 is more straightforward – there is no reason to extrapolate to areas outside the ACS field of view. At the $V < 25.5$ mag cut-off we observe 30 ± 7 per cent of the GCLF, assuming the GCLF turnover is at -7.4 ± 0.2 mag and $\sigma = 1.2 \pm 0.2$ mag. Taking the completeness fraction as 0.95 ± 0.05, we obtain $N_{\rm total} = 67 \pm 23$ and $S_N = 0.6 \pm 0.2$ for 31AC ($M_{\rm V} = -20.5$), $N_{\rm total} = 35 \pm 14$ and $S_N = 1.0 \pm 0.4$ for 31B ($M_{\rm V} = -18.9$), and $N_{\rm total} = 28 \pm 13$ and $S_N = 0.7 \pm 0.3$ for 31G ($M_{\rm V} = -19.0$).

4.3 HCG 42

4.3.1 Globular cluster candidates

The HCG 42 group consists of four large galaxies, three of which are elliptical and one lenticular, with low overall H I content. In the evolutionary sequence scheme this group qualifies as Type III. More details on this group configuration including the dwarf galaxy population can be found in Konstantopoulos et al. (2013). Because of the predominance of elliptical galaxies in the group and the

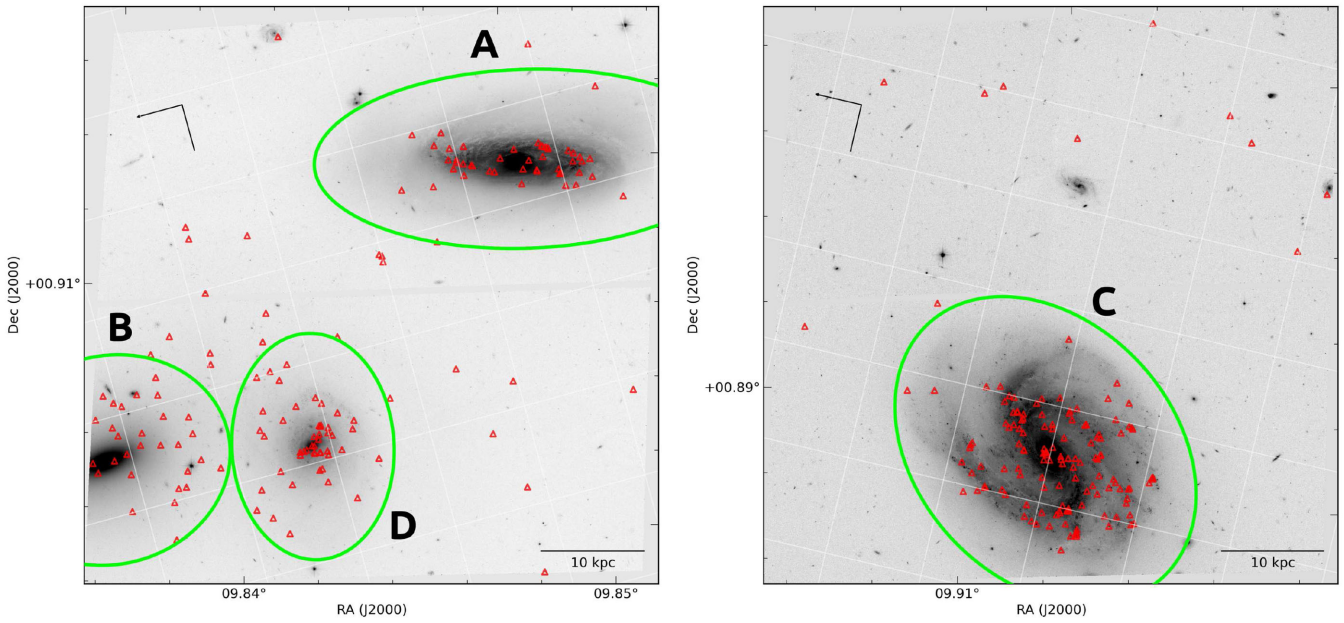

(b) (c)

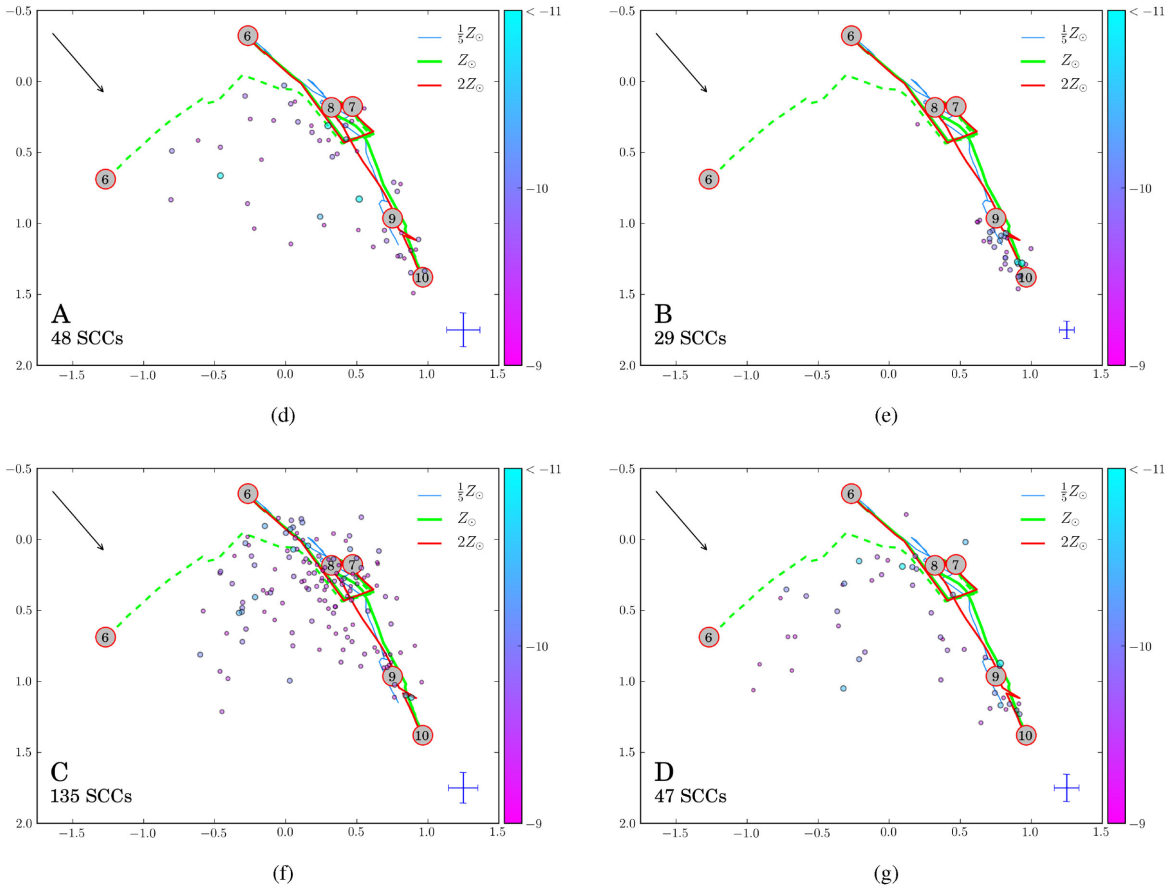

(d) (e) (f) (g)

Figure 6 – *continued*

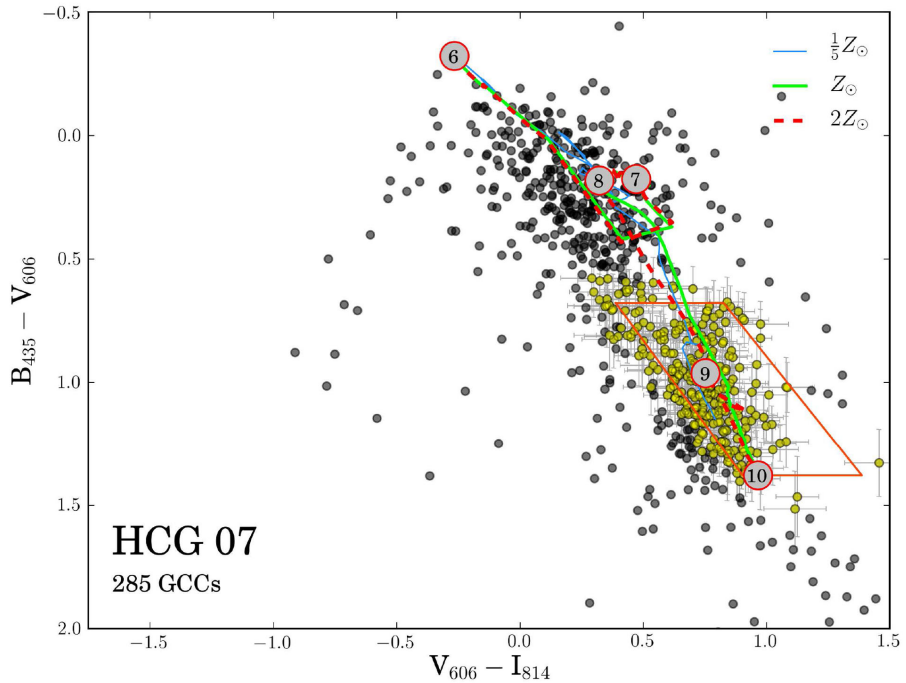

(a)

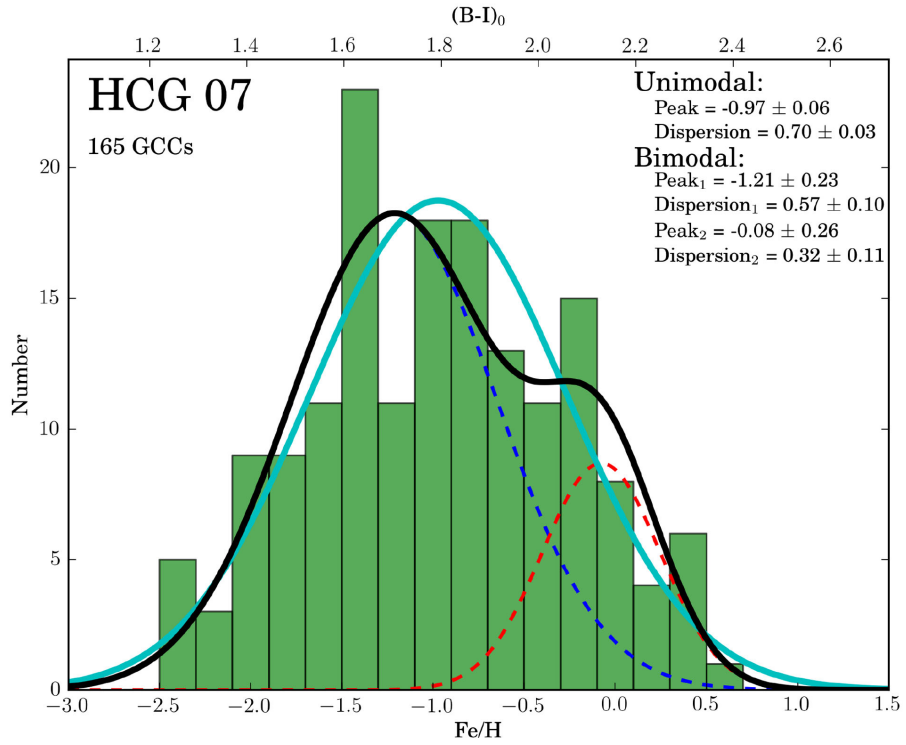

(b)

Figure 7. A colour–colour diagram of all detected GCCs in HCG 07 (a), including clusters located in the IGrM, and their metallicity distribution (b). The selection parallelogram in (a) is based on the colours of Milky Way Globular Clusters (Harris 1996). The number of GCCs in the lower left corner is the number of clusters that are located inside the selection parallelogram or that overlap the selection region with their 1σ error bars. The thin solid line, solid line, and dashed line trace the evolution of SSP models of [0.2, 1.0, 2.0] $Z_\odot$ (Marigo et al. 2008). The numbers on the track denote age represented in log (age/yr). Note that the measured quantity for the panel (b), and for the rest of the plots of the same nature, is the colour index $B - I$. It was converted to Fe/H values according to prescription in Harris et al. (2013) and further analysis were carried out with those Fe/H values. Panels (c) and (d) are inverted V_{606} images which show the GCC system extent, with locations of GCCs overplotted as circles. GCCs found in the central regions and spiral arms of galaxies A and C could potentially be reddened young SCs. Panels (e) and (g) are colour–colour plots for particular galaxies in the group. The systems of 7B and D are considered together because of the projected overlap of their expected GC system extents. Their metallicity distribution is consistent with a single-peaked Gaussian.

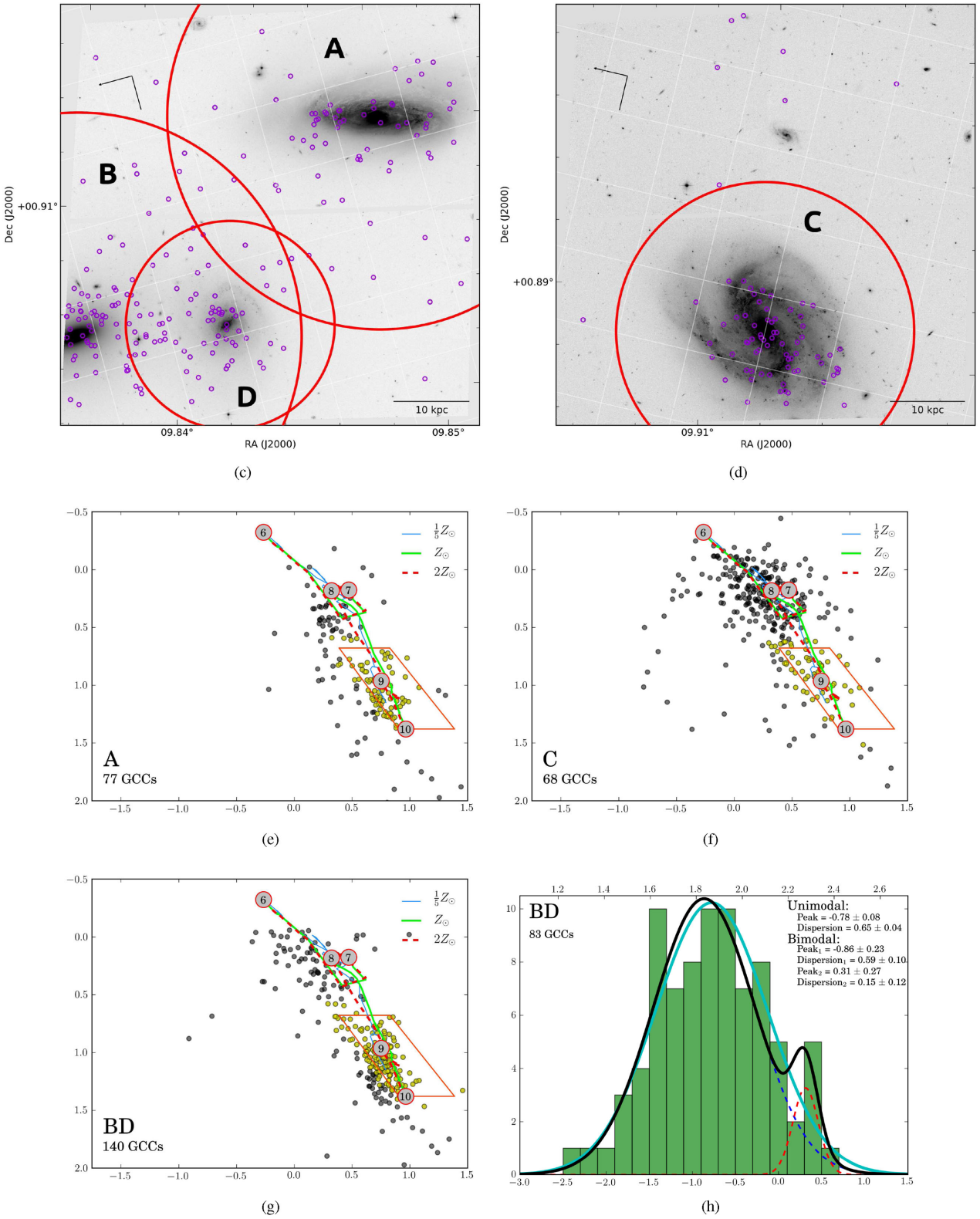

Figure 7 – *continued*

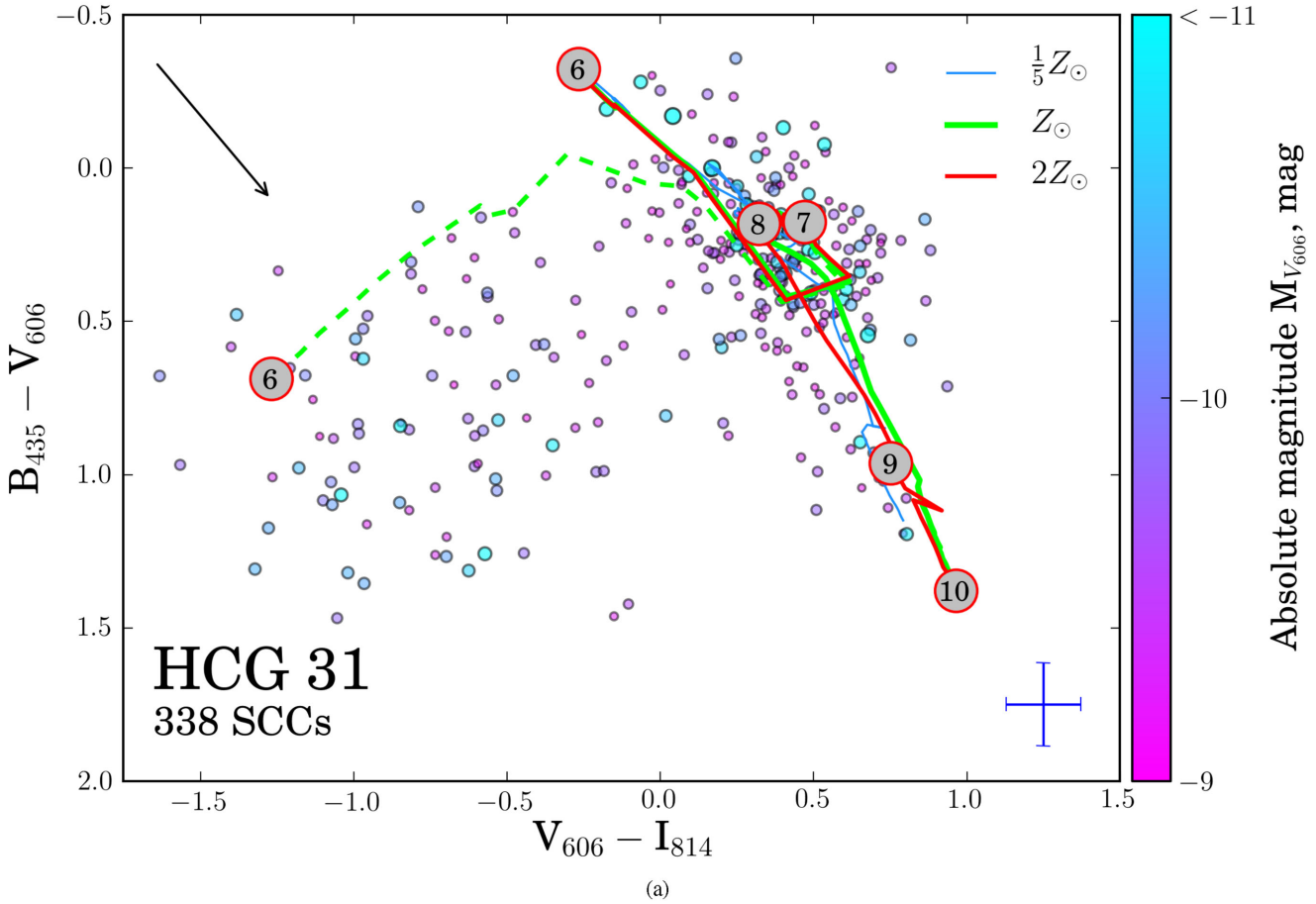

Figure 8. A colour–colour plot of all the SCCs in HCG 31 (a), including clusters located in IGM. Symbols are as in Fig. 6. Image (b) is the inverted V_{606} image which shows the SCC system extent as defined by a brightness contour of $\sim 1.25\sigma$ in V_{606} above the background level. Panels (c)–(f) are colour–colour plots for particular galaxies and regions in the HCG 31 group. All galaxies (31AC, 31B, and 31G) and tidal regions (31E and 31F) in this group host young clusters; the entire system is suffused with star formation triggered by strong, recent galaxy interactions. A colour–colour plot for the galaxy G.

low content of the cold gas, we do not expect to find young and intermediate-age SCs, as illustrated by Fig. 10 panel (c). Thus, we start our SC population analysis by looking at the GCCs. The ACS observations of this group consist of only one pointing that covers the two elliptical galaxies, 42A and 42C (panel b of Fig. 10). The brightest of these two galaxies, 42A, has an optical luminosity comparable to M87 ($M_{\rm V,\,42a} = -22.8$ and $M_{\rm V,\,M87} = -22.77$; Misgeld & Hilker 2011). The extent of the GC system for this galaxy covers most of the field of view and overlaps the extent of the GC system of the neighbouring galaxy 42C. From the magnitude difference of these two galaxies ($M_{\rm V,42c} - M_{\rm V,42a} = 2.11$ mag), most of the detected GCCs in this image are expected to belong to 42A. Additionally, northwards of 42A lies a dwarf galaxy [VC94] 095753−1922.2, which has been identified as a member of HCG 42 (Carrasco, Mendes de Oliveira & Infante 2006; Konstantopoulos et al. 2013). We observe a slight overdensity of GCs in that region (panel c of Fig. 11). However, following the same line of argument as above, we consider those clusters to be part of the 42A GC system. Altogether, there are 878 detected GCCs that located inside the GC system extent. The photometric metallicity distribution as probed by $B_{435} - I_{814}$ was determined for 393 of them (for reasons mentioned in Section 3.5). The distribution has a very well defined bimodality with peaks at [Fe/H] $= -1.04 \pm 0.07$ and [Fe/H] $= 0.16 \pm 0.15$, for the 'blue' and 'red' peaks, respectively. Both peaks appear to be more metal rich by ∼0.4 as compared to the average peaks of GC metallicity distributions of approximately −1.5 and −0.5 measured for different types of galaxies (VanDalfsen & Harris 2004, and references within).

From RC3, we find that the effective radius is 32.9 arcsec (estimated from a Johnson *B* image and corresponding to ∼9.4 kpc); the value for the velocity dispersion of 321.4 ± 9.3 was obtained from HyperLeda (Makarov et al. 2014).[4] Using the above numbers and equation (4), we find that the predicted population of the GC system for 42A is 2498 ± 146 GCs. At the cut-off magnitude of $M_{\rm V} = 25.0$ and with the assumption for GCLF turnover at -7.4 ± 0.2 mag and $\sigma = 1.2 \pm 0.2$ mag, we probe 14 ± 7 per cent of the GCLF. Taking a completeness fraction as 0.95 ± 0.05, we estimate $N_{\rm total} = 3420 \pm 1710$ and $S_N = 2.6 \pm 1.3$. Although the $N_{\rm total}$ number is ∼50 per cent larger than one predicted by equation (4), it is still within reasonable uncertainties. Given the large number of GCCs in a luminous, central dominant group elliptical, it seems likely that 42A is the product of a gas-rich merger from several Gyr ago.

[4] http://leda.univ-lyon1.fr

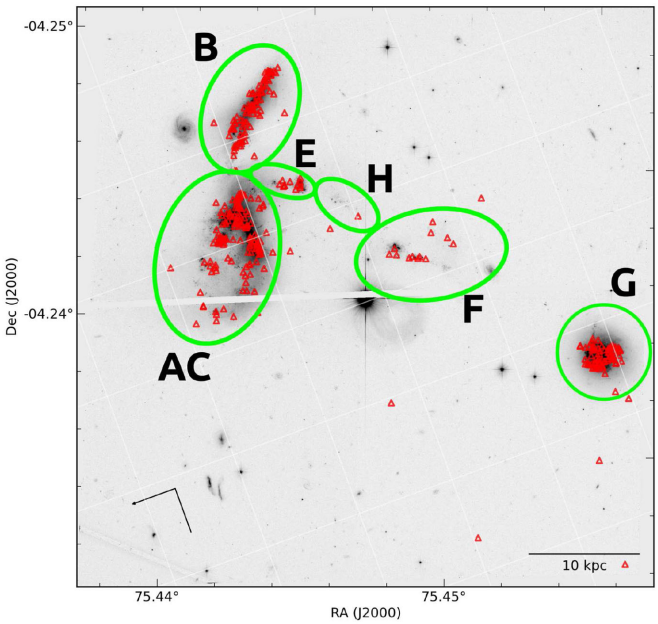

(b)

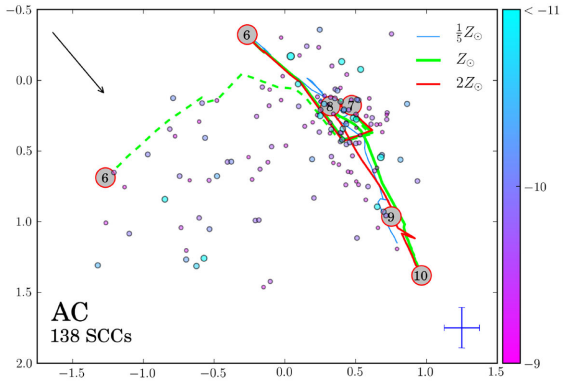

(c)

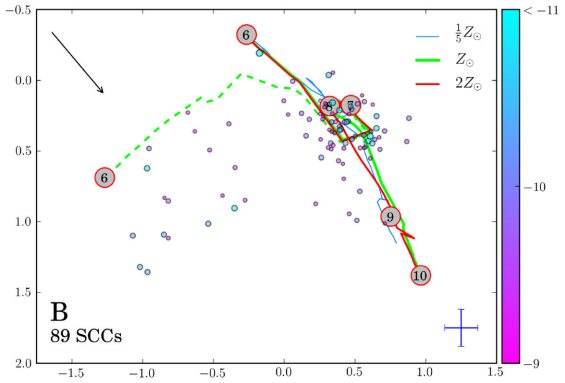

(d)

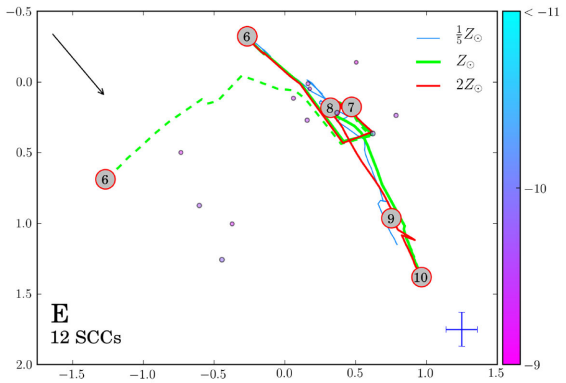

(e)

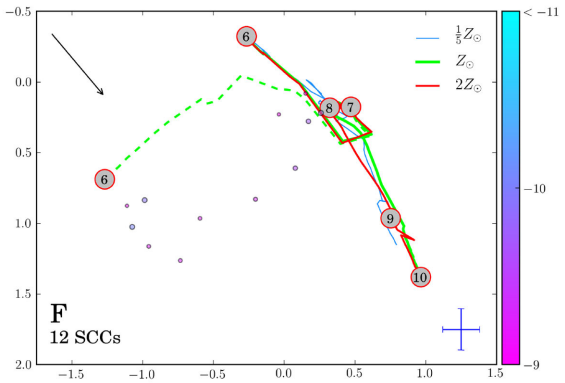

(f)

Figure 8 – *continued*

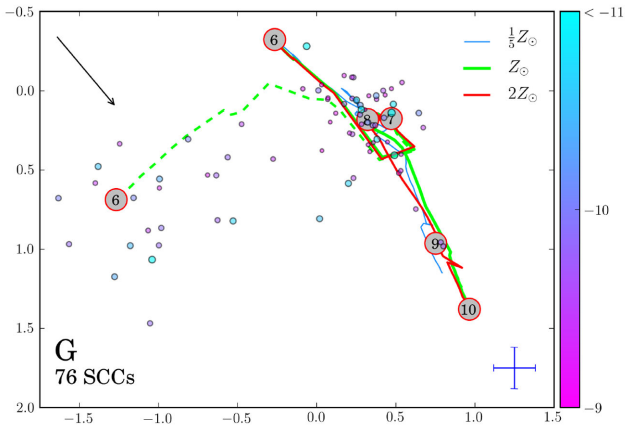

(g)

Figure 8 – *continued*

4.4 HCG 59

4.4.1 Star cluster candidates

According to Konstantopoulos et al. (2012), HCG 59 belongs to the Type III groups, with low H I content relative to its apparent dynamical mass. However, a number of young SCCs are found in this group, located in the smaller galaxies 59C and 59D (panels f and g of Fig. 12). The SCC population of the spiral 59C is somewhat small, with only 16 SCCs detected in the disc of the galaxy. These clusters span a range of ages between a few Myr and 1 Gyr, similar to clusters in the large irregular 59D. The difference between the SCC populations of those galaxies is that 59D has a larger population of clusters detected and there is also a number of very young clusters present (∼1 Myr). Given that these two galaxies have approximately the same stellar mass (Table 2), we can compare their specific SFRs (sSFRs) and see that 59D is forming stars over eight times more efficiently than 59C (sSFRs are 0.024 and 0.200 Gyr^{-1} for 59C and 59D, respectively), which can be seen clearly in the colour–colour plots for each galaxy. The irregular galaxy 59D has a higher sSFR likely because of the larger amount of available cold gas. Star formation in 59D may also be enhanced dynamically because of its proximity to 59A.

4.4.2 Globular cluster candidates

The majority of GCCs in HCG 59 are part of the GC system of the elliptical galaxy 59B (IC 0736) (panels d and g of Fig. 13). Intriguingly, it appears that the GCC population is much richer than would be expected of a galaxy of its luminosity ($M_B = -18.5$; Sabater et al. 2012). We use the SDSS (York et al. 2005) values for the velocity dispersion, $\sigma = 99.9\ \mathrm{km\,s}^{-1}$ and the value of the effective radius $R_\mathrm{e} = 3.18$ arcsec (as determined from a deVaucouleurs profile) which corresponds to 0.96 kpc. Substituting these numbers into equation (4), we find that the predicted number of GCs for this galaxy $N_{\mathrm{GC,pred}} = 29 \pm 2$ is significantly smaller than the number of GCs estimated from the observed bright end of the GCLF ($N_{\mathrm{total}} = 507 \pm 150$, details to follow), and is in fact even smaller than the number of detected GCCs ($N_{\mathrm{All\ GCCs}} = 191 \pm 14$ or $N_{95\ \mathrm{per\ cent}} = 112 \pm 11$ for sources with 95 per cent completeness level). However, we note that the velocity dispersion value taken from SDSS appears to be rather low for a galaxy with this mass (see Table 2). In addition, we point out the unusually dense population of extragalactic SCs located to the south-west of 59B (panel d of Fig. 13), away from the visual centre of the group and along the stellar stream that appears to connect galaxies A and B (Konstantopoulos et al. 2012). One of the possible explanations for this population of clusters is that they are possibility a remnant of a prior interaction between the A and B galaxies, approximately 1 Gyr ago (see Konstantopoulos et al. 2012 for further discussion).

At the cut-off magnitude of $M_\mathrm{V} = 25.5$ and with the assumption of a GCLF turnover at -7.4 ± 0.2 mag and width $\sigma = 1.2 \pm 0.2$ mag, we probe 22 ± 6 per cent of the GCLF of galaxies in this group. Taking the completeness fraction as 0.95 ± 0.05, we estimate $N_{\mathrm{total}} = 86 \pm 33$ and $S_N = 0.7 \pm 0.3$ for 59A ($M_\mathrm{V} = -20.1$; after removing clusters around the irregular 59D that are within the expected 59A GC system extent, but are most likely reddened young SCs), and $N_{\mathrm{total}} = 507 \pm 105$ and $S_N = 8.7 \pm 2.6$ for 59B ($M_\mathrm{V} = -19.4$). For galaxy 59C, the number of detected GCCs from the 95 per cent completeness subcatalogue, is on a par with the number of contaminating sources, $N_{\mathrm{obs}} \leq 2$. That gives us the upper limits for $N_{\mathrm{total}} < 10$ and $S_N < 0.1$. We did not estimate N_{total} and S_N for 59D because the detected objects may well be reddened bluer objects, rather than GCCs.

Being the only elliptical with sufficient number of GCCs in this group, 59B was checked for bimodality in its metallicity distribution. The GMM statistical results do not support the idea of bimodality, rather, it would appear that the distribution is unimodal with a peak at $[\mathrm{Fe/H}] = -1.04 \pm 0.05$.

In all, the population of old clusters in HCG 59 is intriguing enough to warrant further study.

4.5 HCG 92

4.5.1 Star cluster candidates

HGC 92, which also known as Stephan's Quintet and which classified as Type II in the proposed CG evolutionary sequence (Konstantopoulos et al. 2010), is a group of five galaxies (including the foreground interloper NGC 7320) with numerous signs of past and ongoing interactions. Another galaxy associated with the group, NGC 7320C, is not in the *HST* field of view. As a result, this group exhibits the largest number of detected SCs in our sample. There are a number of interesting features singular to this group which are explored in depth in Fedotov et al. (2011). For example, we were able to detect SCs in two tidal tails, the Old Tail (OT) and Young Tail (YT) – Fig. 14. Because tidal tails typically have low gas and dust content ($A_V \lesssim 0.5$ mag; e.g. Temporin, Staveley-Smith & Kerber 2005), SCs in tails usually suffer minimal reddening and their ages estimated from *BVI* colour–colour plots are more accurate than in galaxy discs. In our case, SCs detected in these tails have compact distributions in the colour–colour plane, supporting the idea that SCCs within each tidal tail were formed coevally (Trancho et al. 2012), presumably during the interactions that caused the formation of those features. Thus, from overdensities of SCs in colour–colour plots and supplemental information from the literature, we were able to estimate the ages for the young and old tidal tails to be 150–200 Myr and 400–500 Myr, respectively (Fedotov et al. 2011).

HCG 92 is an ideal system to study populations of SCs forming outside of galaxies. In particular, there are two areas of extragalactic clusters labelled as the Northern Star Burst Region (NSBR) and the Southern Debris Region (SDR). The NSBR has an SCC population that spans a wide range of ages, from young SCCs of a few Myr

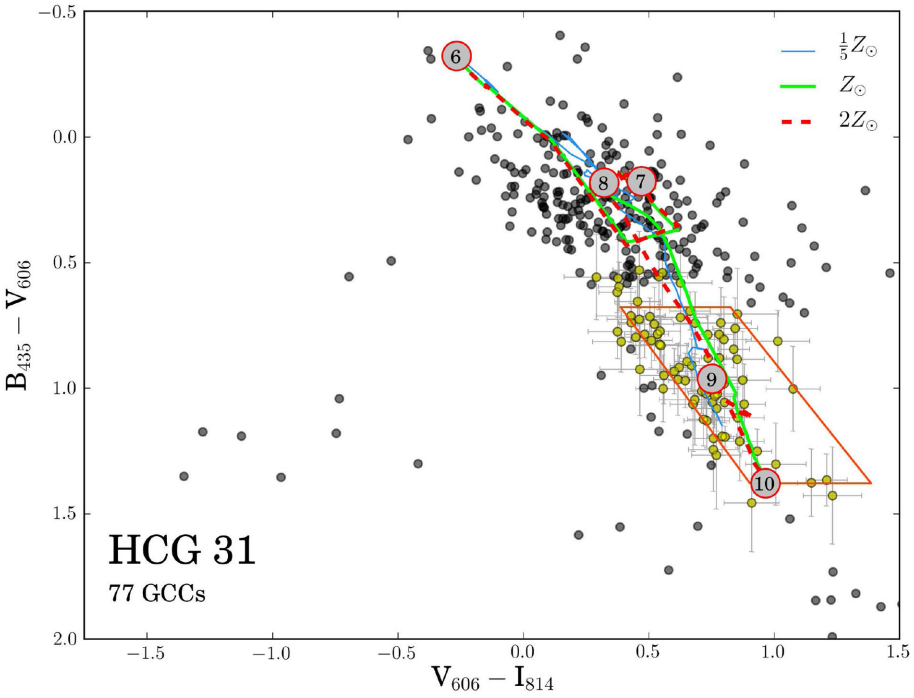

(a)

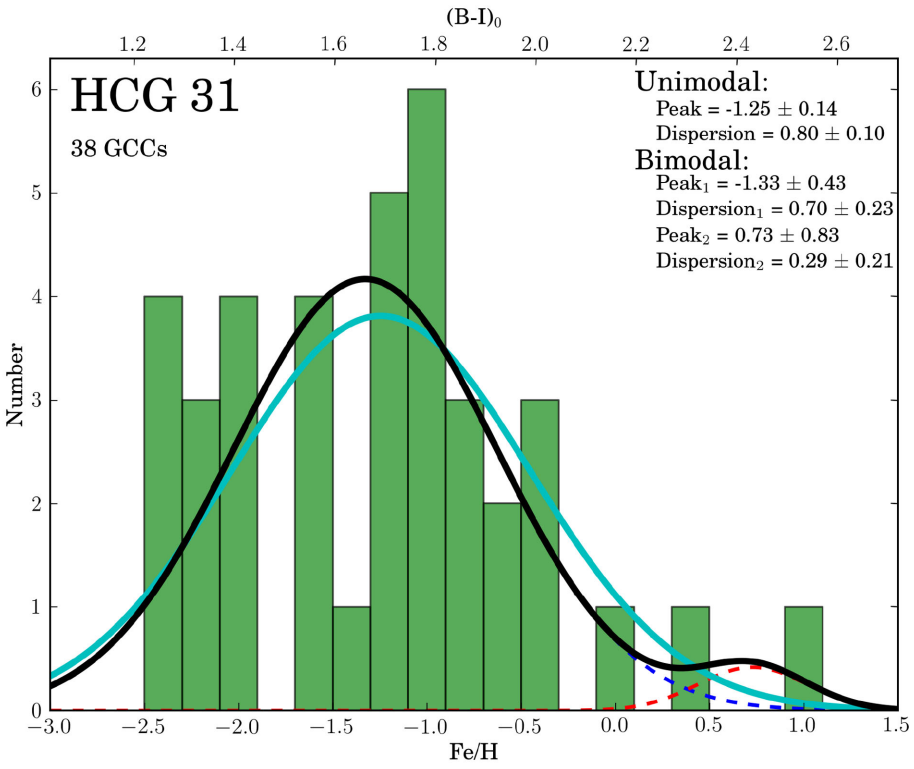

(b)

Figure 9. The GCC population of HCG 31 (a) and its metallicity distribution (b). For more details see caption for Fig. 7. Given the high rate of star formation in this group, the low masses of the individual galaxies, and the spatial distribution of GCCs, it is reasonable to assume that the majority of the SCs labelled as GCCs are in fact reddened young clusters. Therefore, the metallicity distribution plot (b) should be considered with caution. Panel (c) is an inverted V_{606} image which shows the GCC system extent, with locations of GCCs overplotted as circles. Panels (d)–(f) are colour–colour plots for particular galaxies/regions in that group. Most likely, the majority of the small population of GCCs are reddened young clusters.

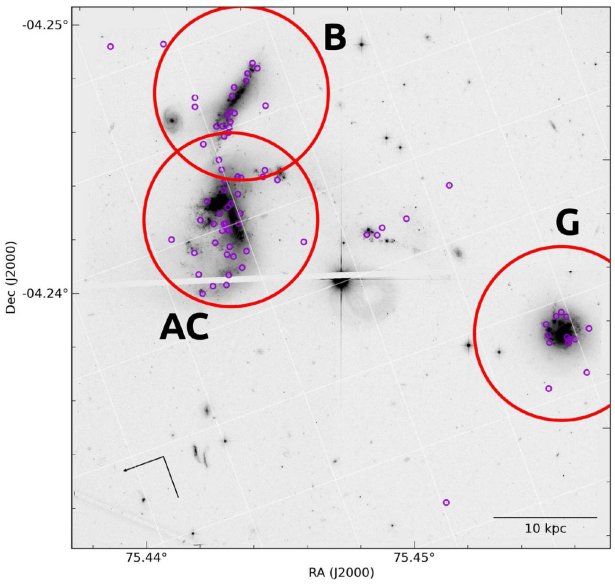

(c)

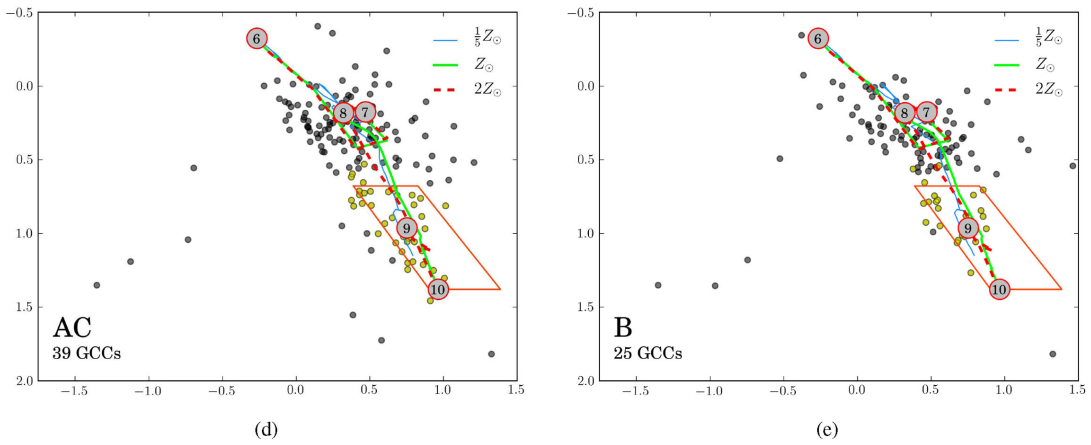

(d) (e)

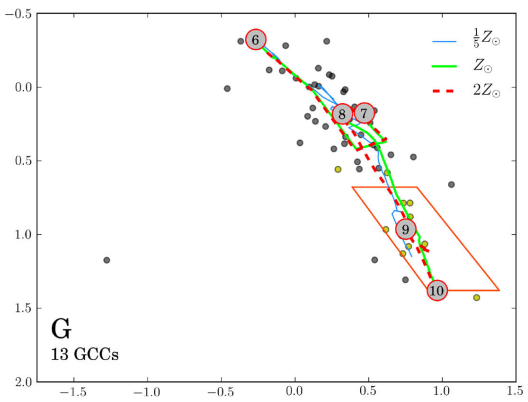

(f)

Figure 9 – *continued*

to very old GCs of over 10 Gyr old. This region includes two intersecting tidal arcs, a byproduct of the interaction between 92B (NGC 7318B) and 92D (NGC 7318A). The young SCs detected in the region were likely formed during that interaction. The presence of a significant number of intermediate-age SCCs (ranging from 100 to 500 Myr old) could be indicative of earlier interactions involving 92C (NGC 7319), NGC 7320C, and perhaps 92D (Moles, Sulentic & Márquez 1997; Xu, Sulentic & Tuffs 1999). And finally, there are a few old SCs likely deposited into that region through gravitational interactions between the galaxies.

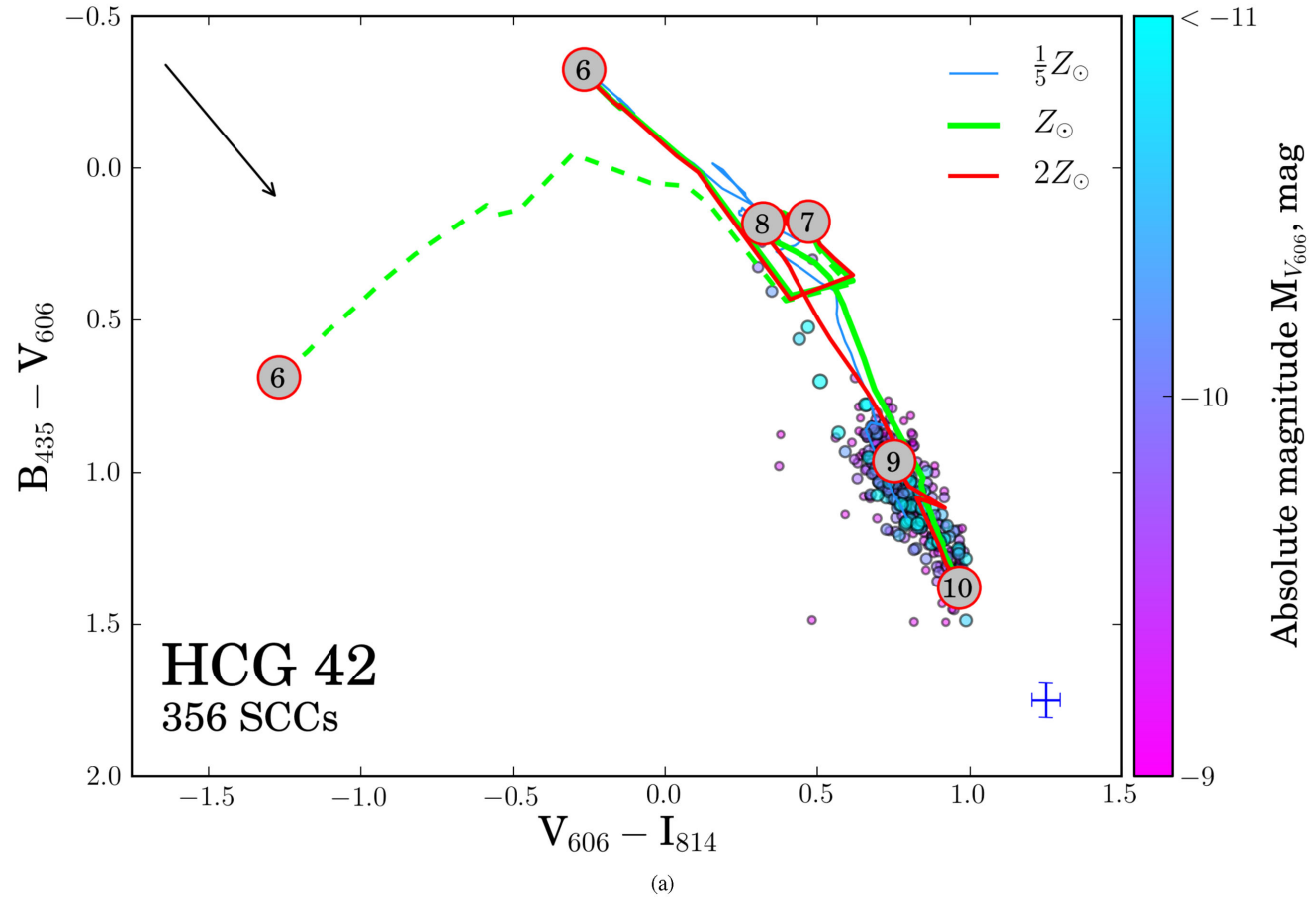

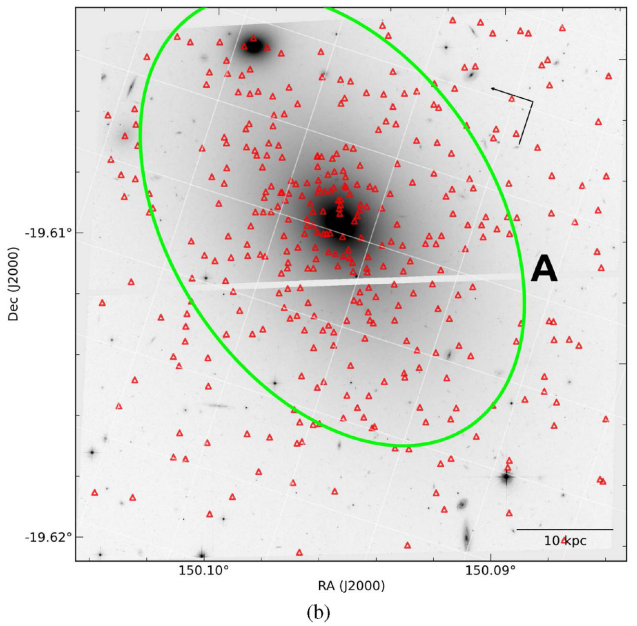

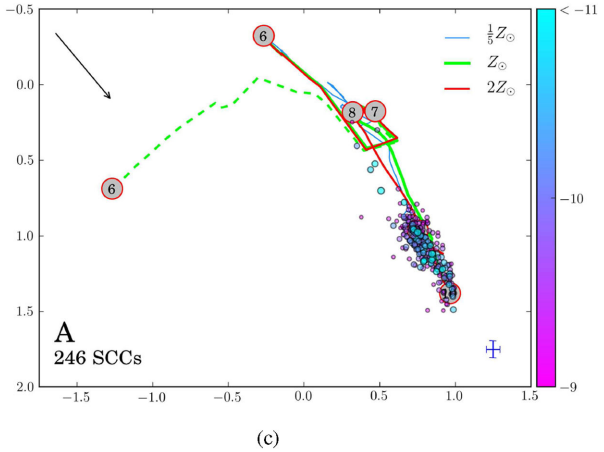

Figure 10. A colour–colour plot of all SC candidates in the ACS image of HCG 42 (a), including clusters in intergroup medium, and subplot for a particular galaxy in that group (b), continued on the next page. For more details see caption for Fig. 6. Panel (b) is the inverted V_{606} image which shows the SCC system extent as defined by the V_{606} brightness contour of $\sim 1.25\sigma$ above the background level. Panel (c) is a colour–colour plot for the luminous elliptical 42A. In this colour-space, all of the clusters are consistent with being old GCs.

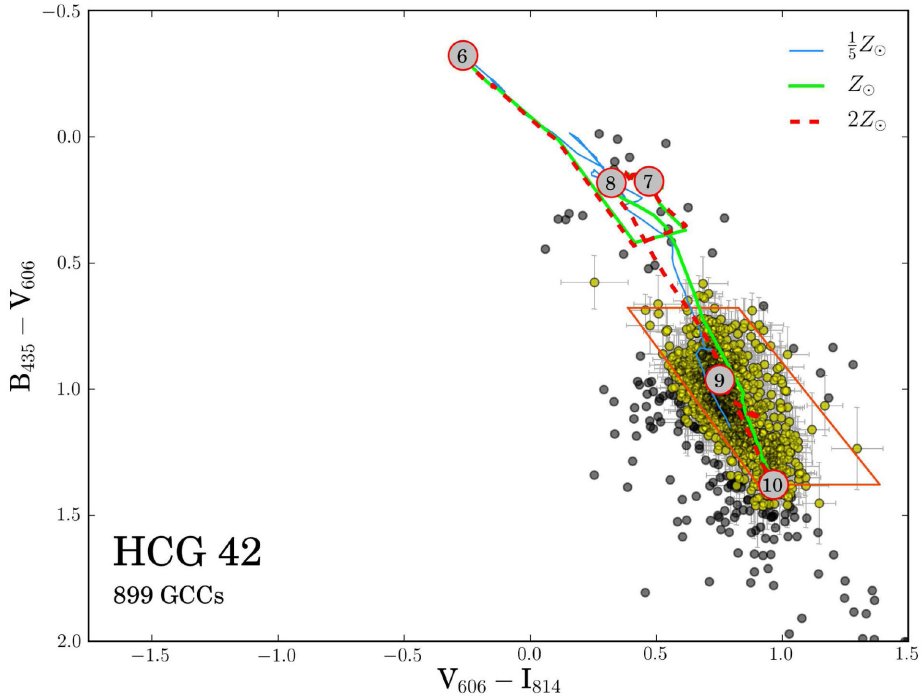

(a)

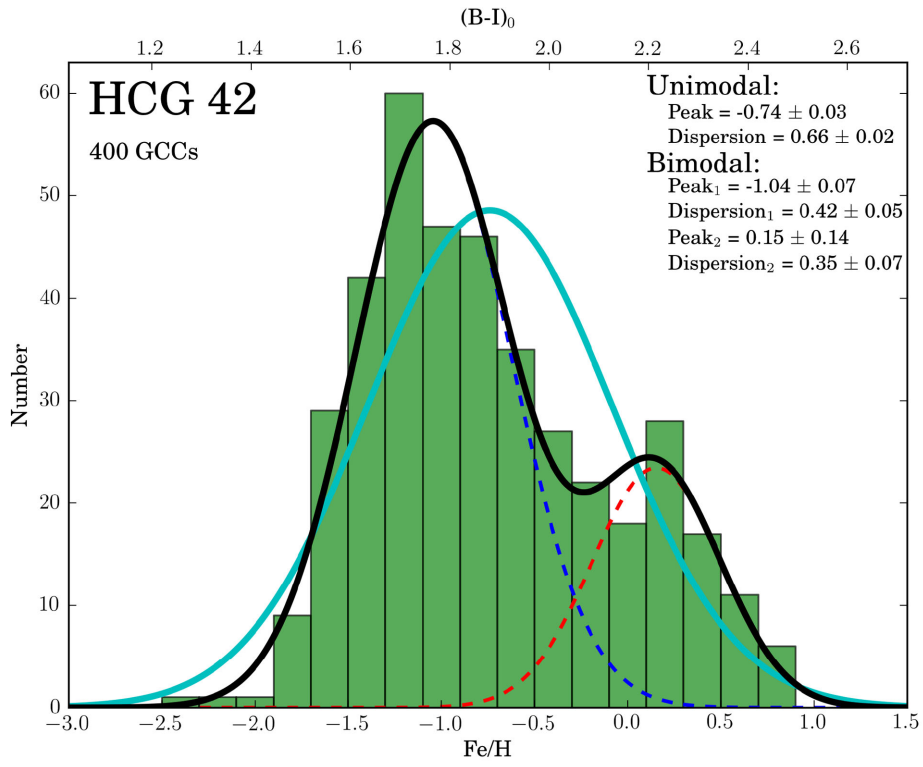

(b)

Figure 11. The GCCc population of HCG 42 (a) and its metallicity distribution (b). For more details see caption for Fig. 7. Panel (c) is an inverted V_{606} image which shows the GCC system extent, with locations of detected GCCs overplotted as circles. Panel (d) is a colour–colour plot for galaxy HCG 42A. A slight overdensity of GCCs close to the left upper corner corresponds to the location of a dwarf galaxy, a member of HCG 42. Panel (e) is a plot of the metallicity distribution of GCCs in HCG 42A. The GMM results favour a bimodal distribution with the first peak at [Fe/H] $= -1.04 \pm 0.07$ and the second peak at [Fe/H] $= 0.16 \pm 0.15$.

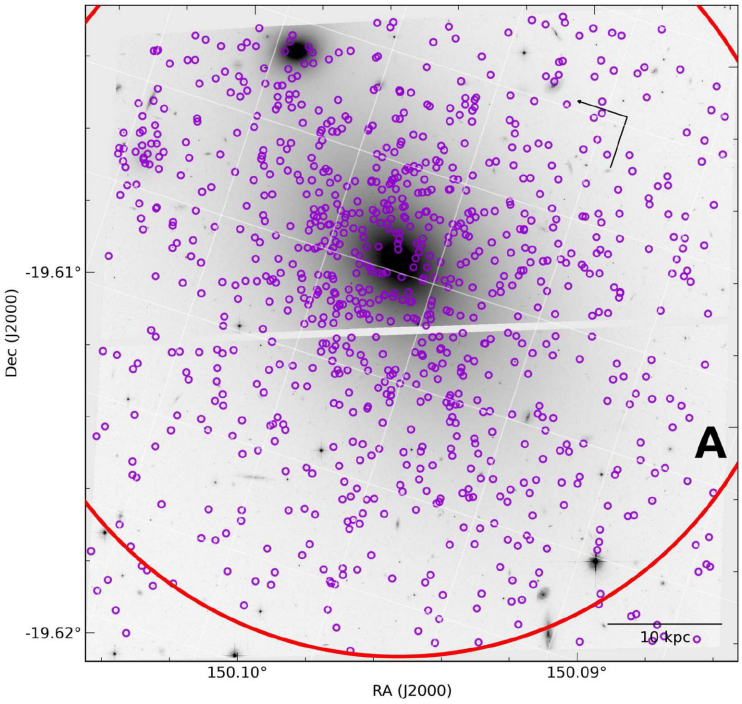

(c)

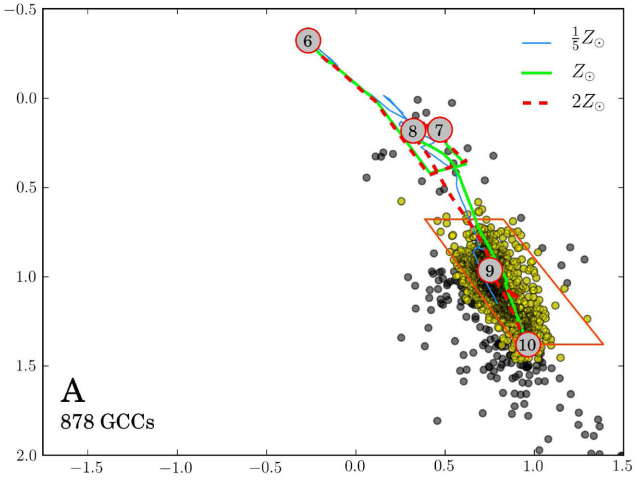

(d)

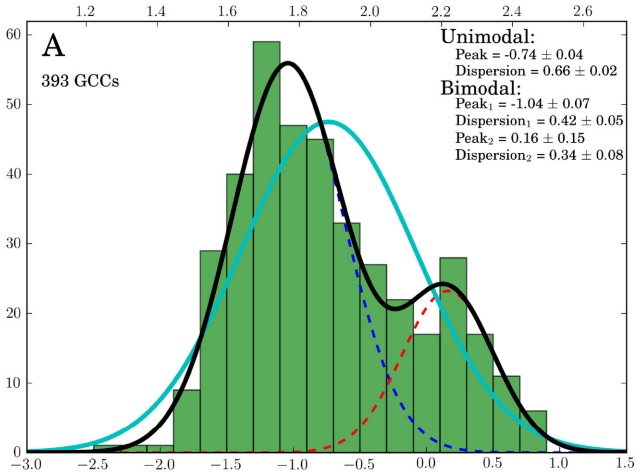

(e)

Figure 11. – *continued.*

Consideration of the SCC population of the SDR, on the other hand, paints a bit different picture. To begin with, there are not as many very young (1–8 Myr) SCs in that region. Also, there is a well-defined separation between two groups of SCCs in the colour–colour plane, one group consists of clusters that are approximately 10–100 Myr old (unfortunately, it is impossible to establish more precise ages based only on *BVI* photometry) and the second group, a collection of older SCs ranging in age from 1 to 10 Gyr. Interestingly, there appears to be a concentration of clusters with ages between 6 and 8 Gyr. Since it is highly unlikely that a galaxy interaction would specifically launch into this extragalactic region SCs of such a limited age range, we speculate that these clusters (with ages 6–8 Gyr) were formed together at some location, and the population of the younger SCCs is either the latest addition or a chance projection. We consider the former as more likely explanation, and as such, SDR could potentially be the remnants of a dwarf galaxy that used up its last reservoir of gas to form these younger population of clusters. However, there are a few reasons why this might not be true. For example, the SDR region appears to extend over a large area for a dwarf galaxy, and there is no detection of extended, diffuse light consistent with a dwarf galaxy.

The spiral galaxy 92C is the largest galaxy in the group. At the same time, it has no detectable H I (Sulentic et al. 2001), which most likely was stripped during previous interactions among the group members (Moles, Marquez & Sulentic 1998). Unless the galaxy manages to acquire more cold gas, the intermediate age

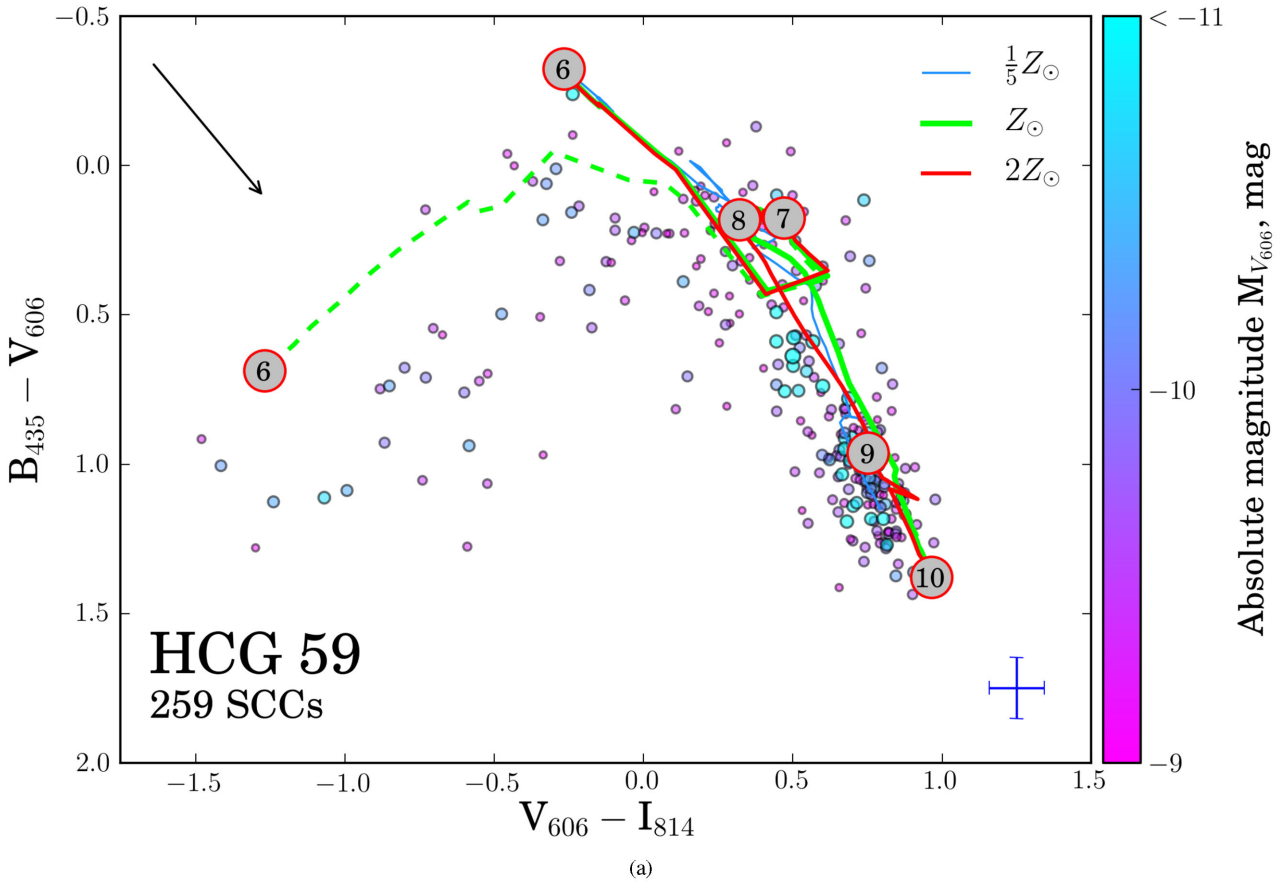

(a)

Figure 12. A colour–colour plot of all SC candidates in HCG 59 (a), including clusters in the intergroup medium, and subplots for particular galaxies in that group (c)–(f), continued on the next page. For more details see caption for Fig. 6. Panels (b) and (c) are inverted V_{606} images which show the SCC system extent as defined by a V_{606} brightness contour of $\sim$1.25σ above the background level. Panels (c)–(f) are colour–colour plots for individual galaxies in the HCG 59 group. The large irregular 59D has a large population of young clusters. 59A hosts both old and intermediate-aged clusters, while the elliptical 59B has only a GC population.

(100–500 Myr) population of SCCs is likely the trace of the last epoch of star formation in that galaxy.

4.5.2 Globular cluster candidates

For the GCC population in SQ, we focus on three regions (panel c of Fig. 15). One region is associated with the elliptical galaxy 92E (NGC 7317), another one with the spiral galaxy 92C (NGC 7319), and the last one with the interacting pair 92B and 92D (NGC 7318B and NGC 7318A). For the last system, we expect that a large fraction of GCCs belong to 92D: first, because it is an elliptical galaxy, and, secondly, it is more massive than the spiral 92B (Table 2). According to our estimates of the GCC system extent, the GCC systems of 92C and 92BD overlap. Moreover, the overlap adds virtually no GCCs to 92BD region, whereas the expected system extent of 92C adds an appreciable part of the eastern tidal feature of 92BD.

According to GMM statistics, the distribution of all GCCs in SQ has detectable bimodality (panel b of Fig. 15). However, the individual distributions for each galaxy/region do not have well defined bimodality, with the possible exception in the case of 92C. However, this galaxy does not have a large enough number of GCCs for statistically significant analysis. If we look at the unimodal peaks of -0.55 ± 0.12, -0.38 ± 0.08, and -0.63 ± 0.10, for the GCC systems in 92C, 92BD, and 92E, respectively, we notice that these values are a bit larger (less negative) compare to the average value of Galactic GCs, the bulk of which have metallicities around [Fe/H] $=-$ 1.3 (Murdin 2001).

4.6 Bimodality of GCC population of elliptical galaxies

Above we discussed bimodality in the galaxies from our sample and the results are outlined in Table 7. We compare our results with those in the literature, in particular, the bimodality analysis in the sample of 92 elliptical galaxies in the Virgo cluster (Peng et al. 2006). The authors found a relationship between the GCs colour distribution modality and absolute magnitude of the host galaxy. According to their fig. 5, which plots the colour distributions of GCs in seven bins of host galaxy magnitude, for the luminous HCG 42A we expect a well-defined bimodality, whereas with the much lower luminosity of HCG 59B, only a weak bimodality is expected. Given that we observe only 22 $\pm$ 6 per cent of the total GC population in that galaxy, it is not surprising that we can-not confirm bimodality of GC distribution. Thus, our findings compare well with the conclusions of Peng et al. (2006): HCG 42A has

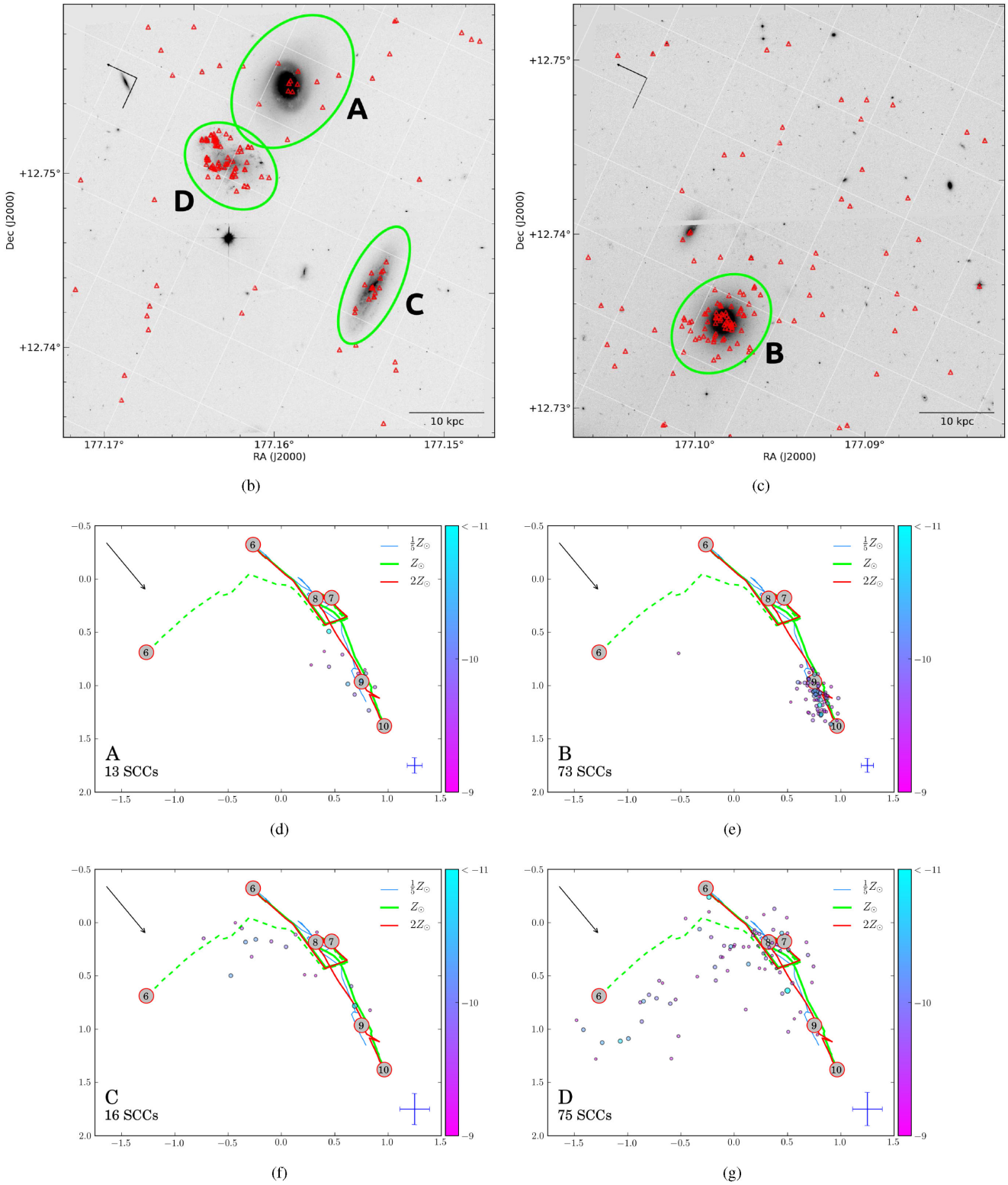

Figure 12 – *continued*

a well-defined bimodal distribution and the colour distribution of HCG 59B GCCs is unimodal. The question of the nature of colour distribution for HCG 92E is still open. The luminosity of HCG 92E, according to Peng et al. (2006), corresponds with a relatively well-defined bimodality. However, we currently do not possess the required number of GCCs to definitively answer that question. As it is, with the currently observed number of GCCs, HCG 92E has a unimodal distribution.

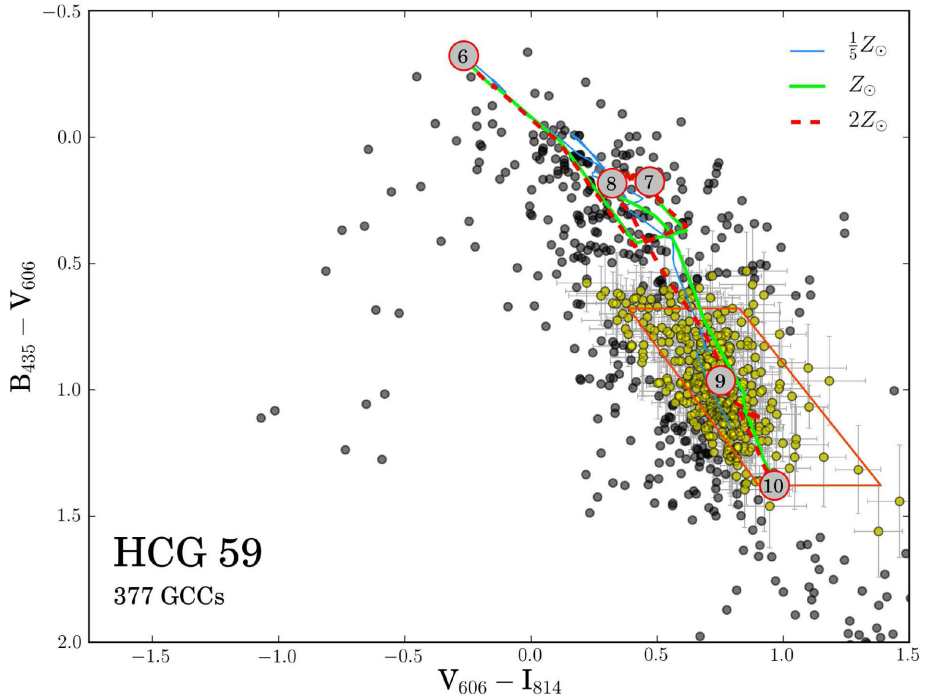

(a)

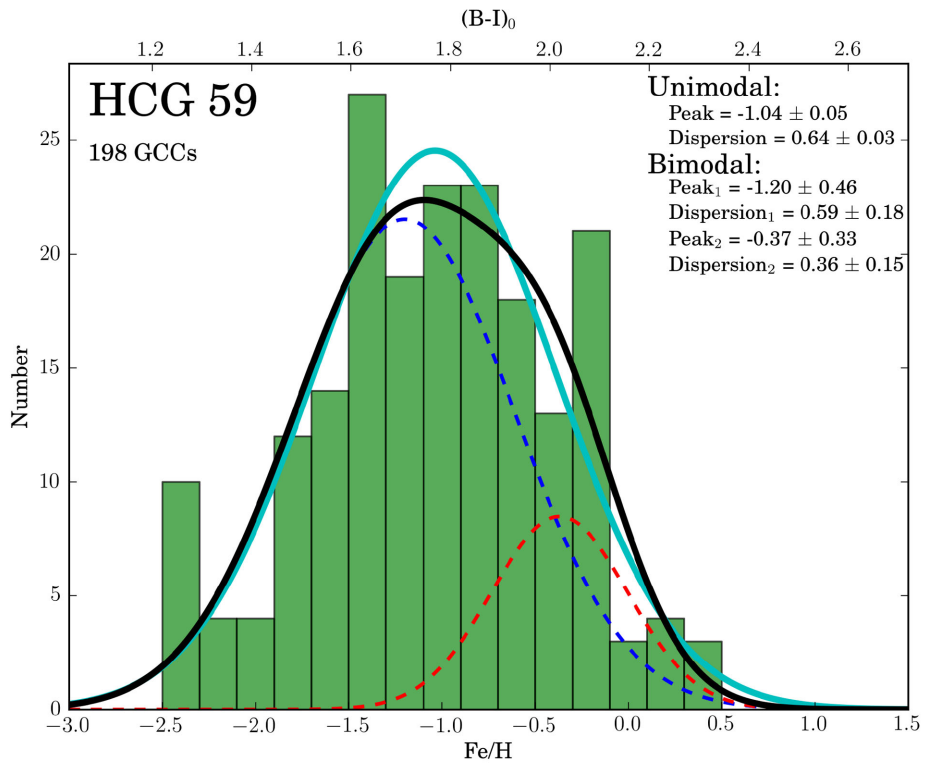

(b)

Figure 13. The GCC population of HCG 59 (a) and its metallicity distribution (b). See caption for Fig. 7. Panels (c) and (d) are inverted V_{606} images which show the GCC system extent, with locations of detected GCCs overplotted as circles. Panels (e)–(g) are colour–colour plots for particular galaxies in that group. Panel (h) represent metallicity distribution of the large population of GCCs in HCG 59B. The GMM results are inconclusive, and a single-peaked distribution is consistent with the data.

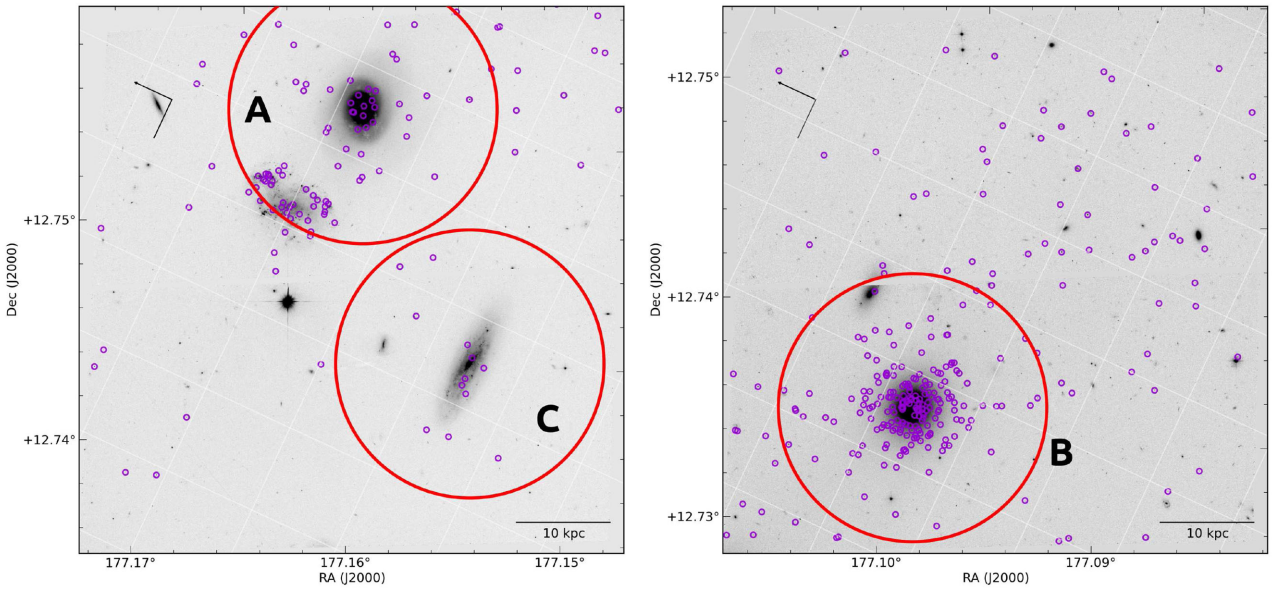

(c) (d)

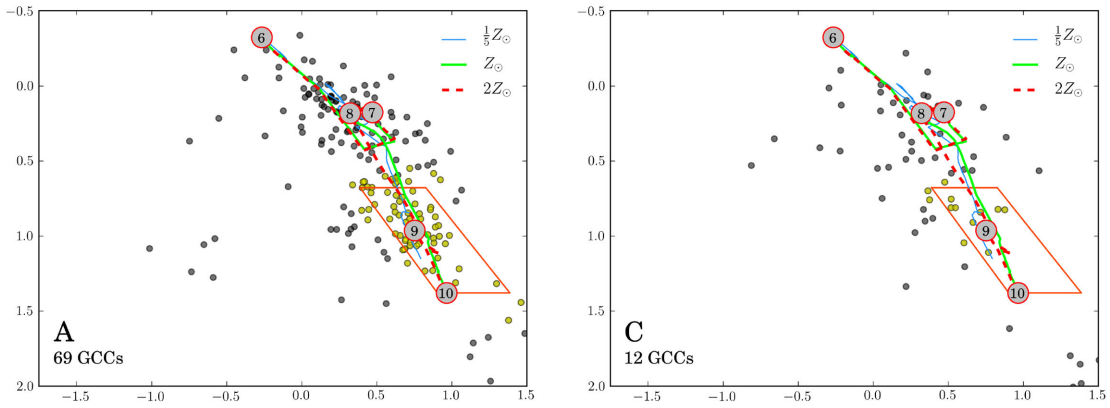

(e) (f)

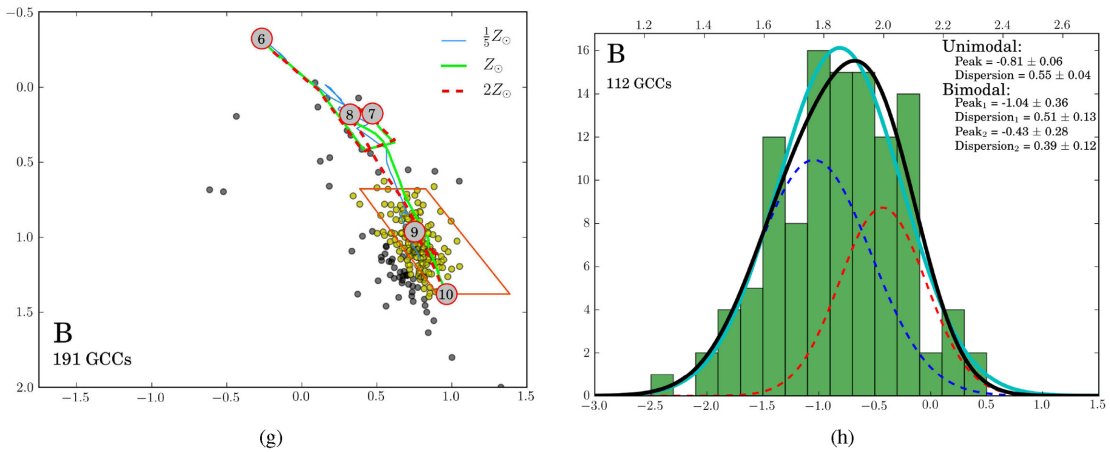

(g) (h)

Figure 13 – *continued*

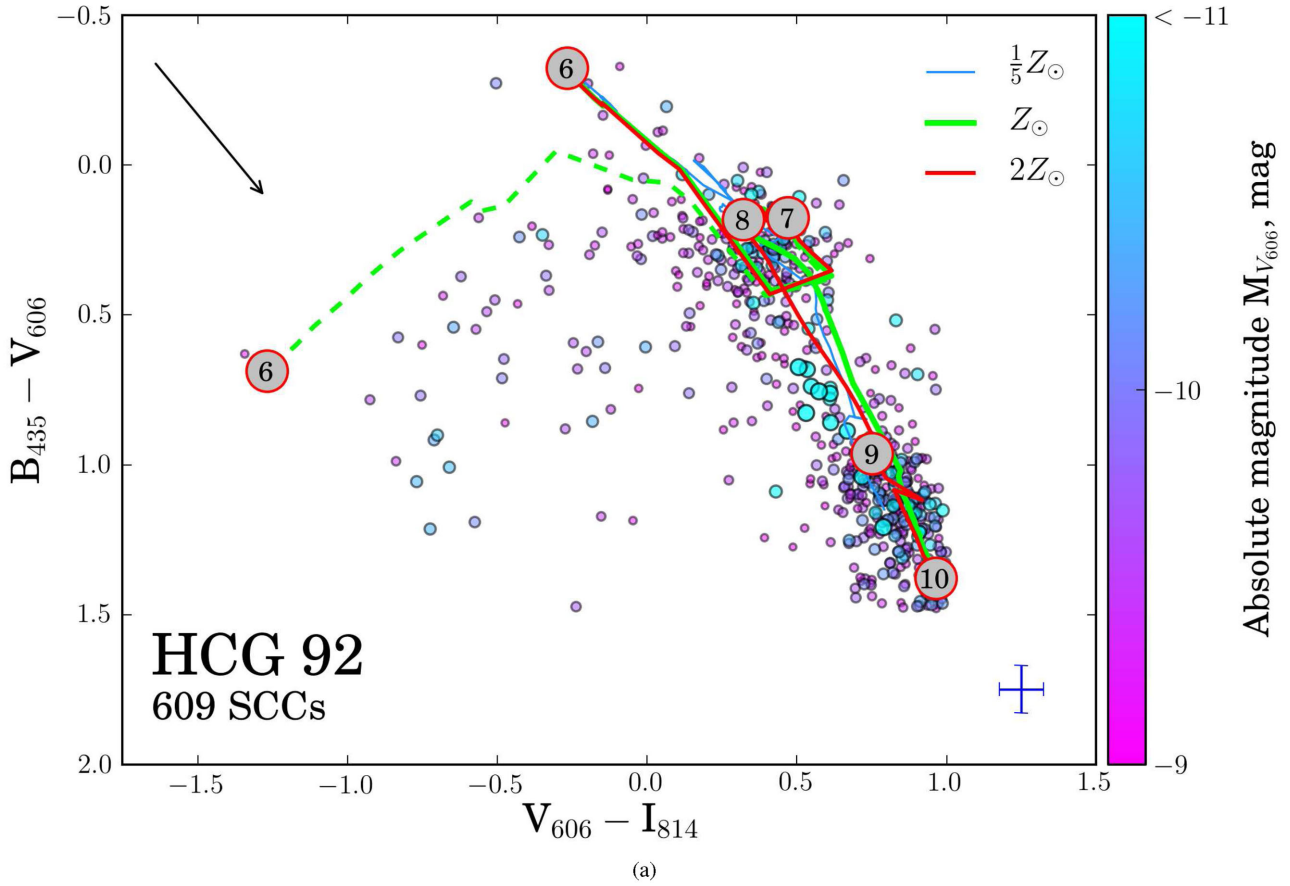

(a)

Figure 14. A colour–colour plot of all SCCs in HCG 92 (a), including clusters in the intergroup medium, and subplots for particular galaxies in that group (c)–(f) and (h)–(i), continued on the next pages. For more details see the caption for Fig. 6. Panel (b) is the inverted V_{606} image which shows the SCC system extent as defined by the V_{606} brightness contour of $\sim$1.25σ above the background level. (The foreground galaxy 92A is outlined in yellow.) Panels (c)–(f) are colour–colour plots for particular galaxies and regions in the HCG 92 group. 92BD has a population of young clusters whose formation was triggered by the collision of 92B with the cold IGM. 92C shows evidence for truncated star formation, with an intermediate (>100 Myr) to old SC population. The Old Tail (OT) and Young Tail (YT) tidal features show small populations of SCs with well-defined colours, tracers of short bursts of star formation in these features. The 8-shape objects observed in the panel (b), also in panel (c) in Fig. 15, are ghost images caused by reflections off the CCD and return reflections from the CCD housing entrance window in WFC3. Panels (g)–(i) are colour–colour plots for particular galaxies and regions in the HCG 92 group. The Northern Starburst Region (NSBR) shows the largest concentration of young clusters within the whole group, the Southern Debris Region (SDR) has a slightly older population of SCs, and the elliptical 92D has primarily old clusters as expected.

4.7 SC populations in CGs

Here, we relate the SC populations to the CG evolutionary sequence proposed by Konstantopoulos et al. (2010, see their fig. 1). Upon inspection, the SCC populations of different group types have qualitative differences. Specifically, the population of HCG 31 (panel d of Fig. 16), classified as a Type I group (gas-rich and dynamically young), is distinguished by a large number of young and intermediate-aged SCs. Type II groups, represented in our sample by HCG 07 and HCG 92 (panels b and e, respectively), still have a large number of young and intermediate SCs; however, a population of >500 Myr to 10 Gyr is also well defined. For CGs of Type III, which predominantly consist of early-type galaxies, we can observe the lack of young SCs, and a significant reduction in the numbers of intermediate-aged SCs (HCG 42, panel f). Initially, Johnson et al. (2007) classified HCG 59 (panel c) as Type II group. The recent work of Konstantopoulos et al. (2013) has associated five additional dwarf galaxies with that group. The updated information on velocity dispersion and H I mass led to a change of the HCG 59 from Type II to Type III. However, based on the observations outlined above, the SC population of HGC 59 would appear to be more consistent with that of Type II groups.

These discrepancies between type classification based on the SC populations and on the ratio of H I to dynamical mass point to the issue of accuracy in measurements of the dynamical masses. In particular, it is quite difficult to accurately measure a dynamical mass of a group given only a handful of radial velocities and the projected separations between galaxies (McConnachie, Ellison & Patton 2008). It may be more appropriate in this case to classify the groups based on the ratio of H I to total stellar mass, which can be much more reliably measured from near-to-mid infrared photometry (Desjardins et al. 2014).

4.8 Cluster luminosity function

Fig. 17 shows the cluster luminosity functions (CLFs) for selected galaxies from our sample. To obtain statistically significant results,

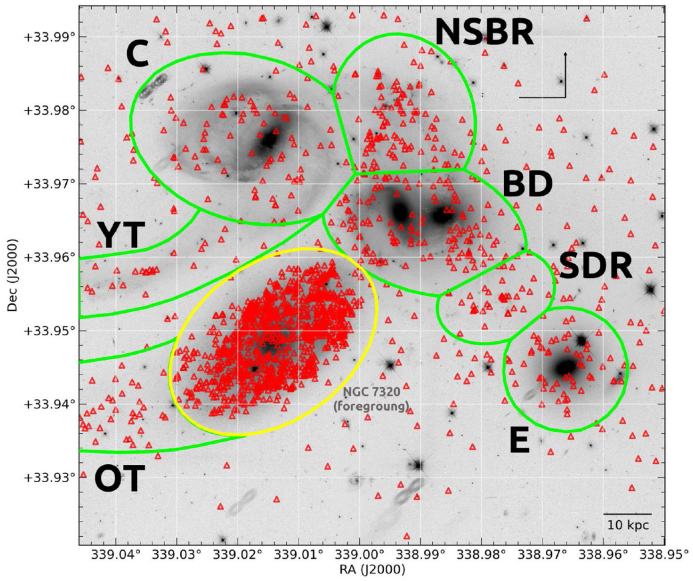

(b)

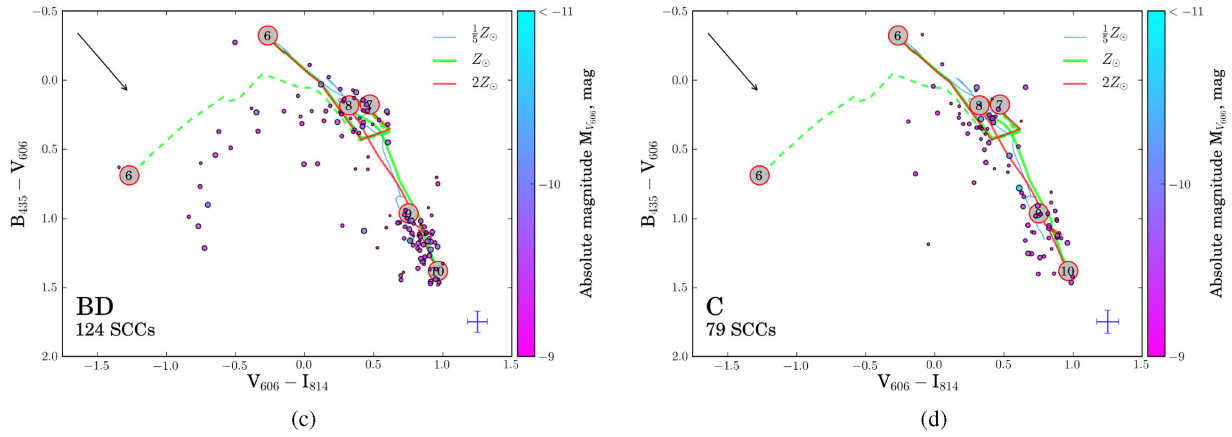

(c) (d)

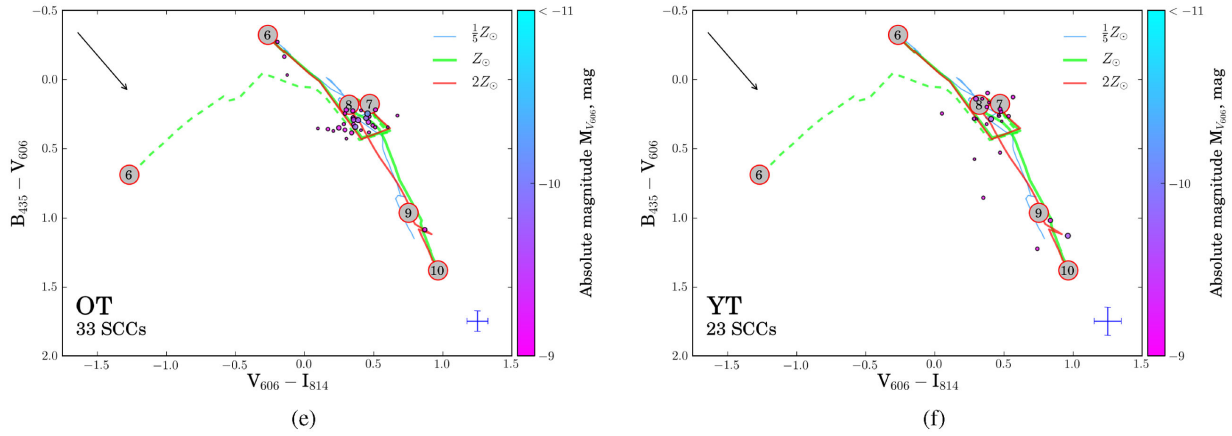

(e) (f)

Figure 14 – *continued*

only galaxies with more than 40 SCCs were used. In each plot, the CLF is shown as a cumulative distribution function of the absolute magnitude, $M_{V_{606}}$. The solid line represents the best-fitting slope of the distribution that was determined by the least-squares fit over the range covered by the line. This range was chosen manually, based on our assessment of the linear region of each CLF starting at the faint-end cut-off. The dashed line represents the best-fitting slope over a common range for all CLFs, from −9 to −10.75 mag. The slope is for a power-law distribution index α from $NdL \propto L^{-\alpha}dL$ as 2.5 × slope + 1. The overall range of the indices (from here on we

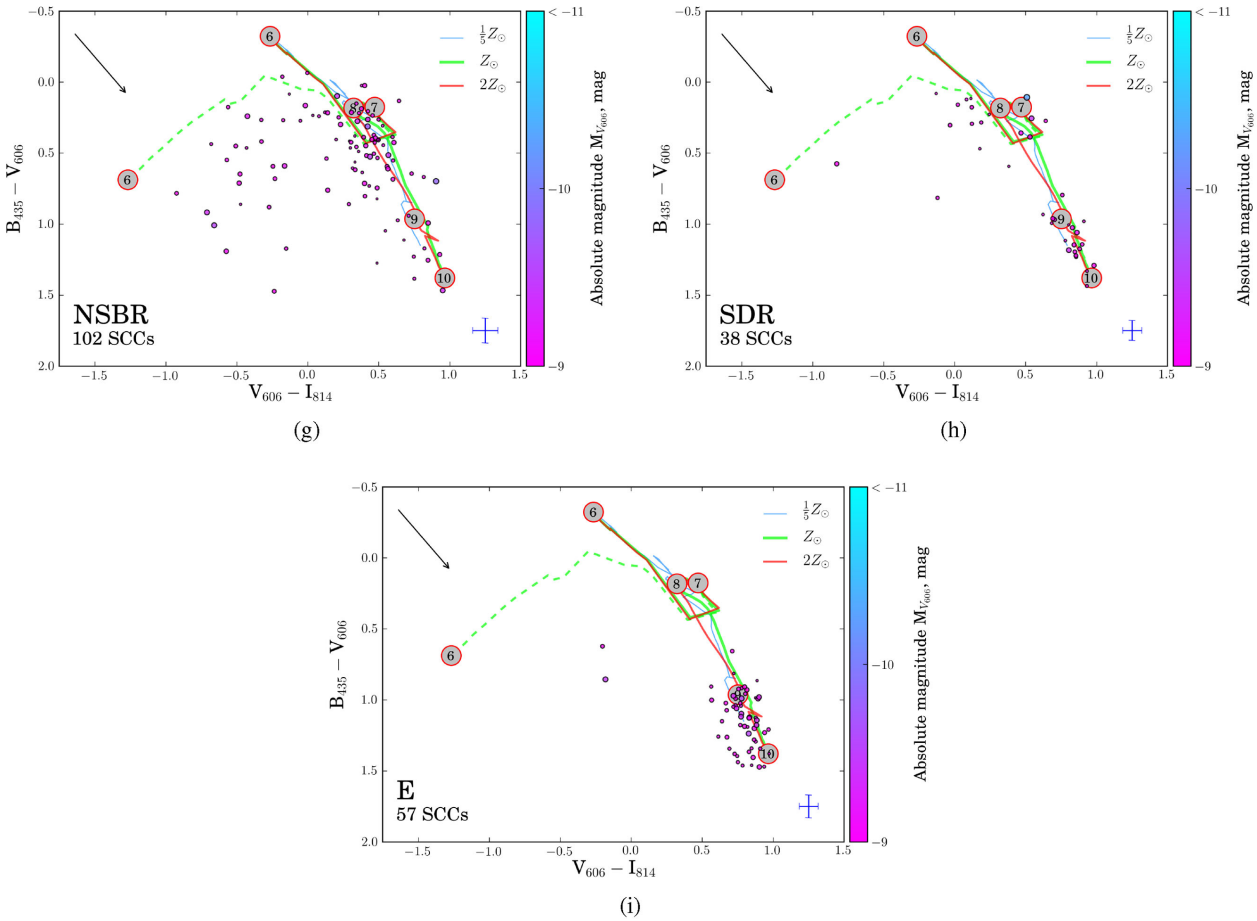

Figure 14 – *continued*

are using slopes fitted to the custom ranges) for CG galaxies in our sample is from −2.13 to −3.24 (see Table 8 for all the numbers). Fig. 18 represents a plot of the LF index as a function of *Hubble* T-type. For comparison, on the same figure, we overplot the data for 20 nearby star-forming spiral galaxies, which span *Hubble* T-types from 2 to 9, obtained from Whitmore et al. (2014). As can be seen, our results do not reproduce the shape of the LF index distribution of Whitmore et al. (2014). Moreover, it appears that no significant correlation between α and T can be observed.

Overall, the CLF indices of spirals in our sample of galaxies are in reasonable agreement with the values reported in other works (e.g. Larsen 2002; Ryon et al. 2014; Whitmore et al. 2014), except for a noticeable outlier 07C, which is a bit more negative than in Gieles et al. (2006). In addition, the galaxies in HCG 31 have very similar α-values (-2.39 ± 0.04, -2.36 ± 0.05, and -2.38 ± 0.05, for galaxies 31AC, 31B, and 31G, respectively); the irregular 59D has a rather high negative α-value of -2.82 ± 0.05. As in the case of 07A and 07C, recent (and ongoing) star formation could be responsible for the steeper value of α in 59D. A sustained star formation episode could cause a build-up of clusters near the low-luminosity end of the LF as old clusters fade with age.

Some CLFs for the galaxies in our sample exhibit a bend at the bright part of the distribution, with that part of the distribution being steeper, a trend that was also noticed in the aforementioned studies. Gieles et al. (2006) argues that the bend in the CLF corresponds to the upper mass limit in the cluster initial mass function. For example, their linear fit to the CLF of the Antennae galaxies suggests a bend at $M_V = -10.3$, which corresponds to a maximum mass of $\sim 2.5 \times 10^6$ $M_\odot$(with the assumption that the oldest cluster in the CLF is 3 Gyr). In our sample, the galaxies 42A, 92BD, 92E display a bend at magnitudes of approximately −10.2, −10.4, and −10.3, respectively. Galaxy 59B exhibits two possible bends, one at −9.5 and the other one at ∼−10.3. Because there is the possibility that the GC system for this galaxy consists of two populations, its own GCs and clusters stripped from 59A (see Section 4.4), we speculate that each bend is imprinted on the overall CLF by the two constituent cluster populations. HCG 31B and HCG 92C might also have multiple bends.

Also worth noting is that the galaxies with active star formation according to the cluster colour–colour plots (in particular galaxies C and D in HCG 07; AC, B, and G in HCG 31, and irregular galaxy D in HCG 59) show the most linear CLFs over a broad range of absolute magnitudes.

4.9 Spatial distribution of GCs in elliptical galaxies

For the three elliptical galaxies in our sample with significant GC systems (HCG 42A, 59B, and 92E), we examined the physical distribution of the GCs in those galaxies as a function of metallicity (Fig. 19). We divided the clusters in each system into three groups, based on their metallicity distribution plots (e.g. panel e

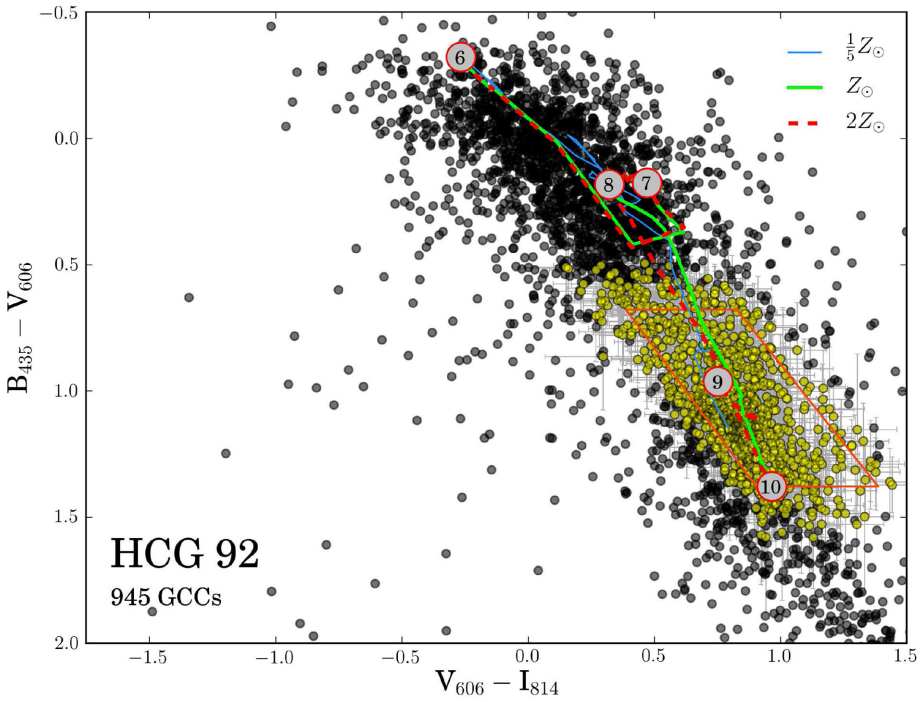

(a)

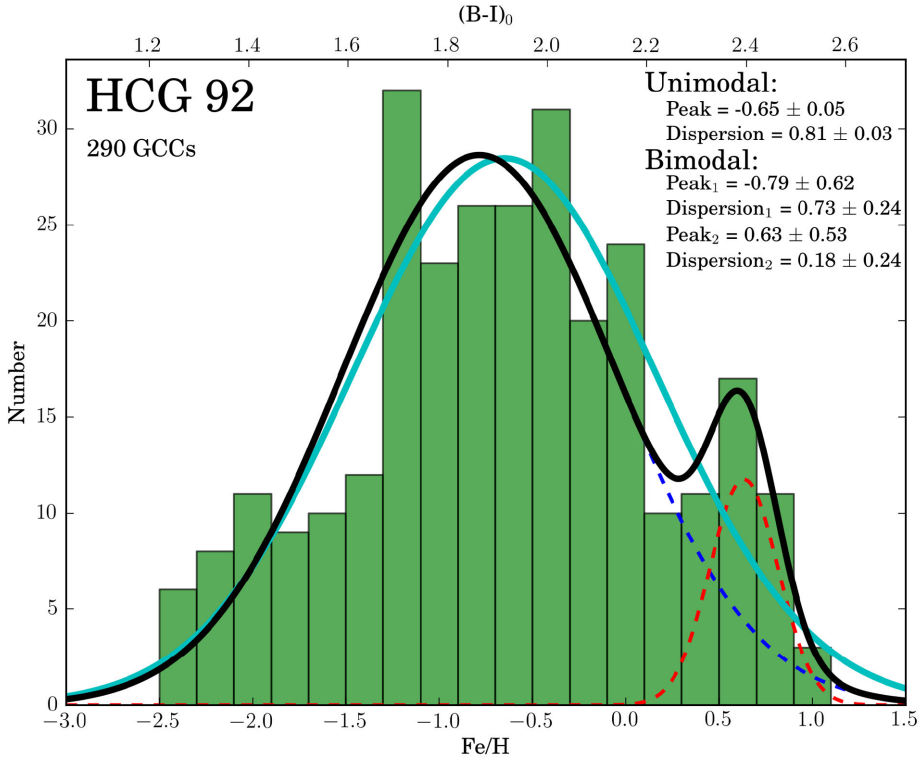

(b)

Figure 15. The GCCs population of HCG 92 (a) and its metallicity distribution (b). See caption for Fig. 7. Panel (c) is the inverted V_{606} image which shows the GCC system extents, with locations of detected GCCs overplotted as circles. Panels (d) and (f) are colour–colour plots for particular galaxies and regions HCG 92. NGC 7319 (HCG 92C) is a face-on spiral and the GCC located in the central region, as well as in the spiral arms, could potentially be reddened young SCs. The BD region contains the elliptical galaxy NGC 7318A (HCG 92D) and the spiral galaxy NGC 7318B (HCG 92B) in a field of debris, material left from current and previous interactions. Thus, it is likely that GCCs in the BD region are heavily contaminated by reddened young SCs. Panels (e) and (g) are the metallicity distributions for C and BD, respectively. Panel (h) is a colour–colour plot for galaxy E and panel (i) is a plot of its metallicity distribution.

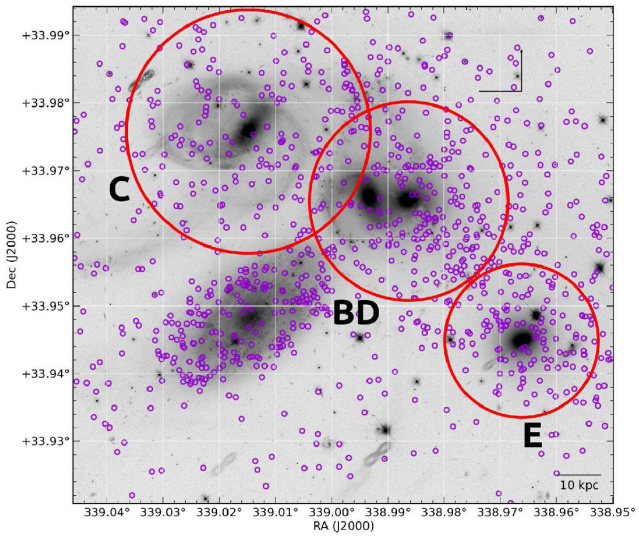

(c)

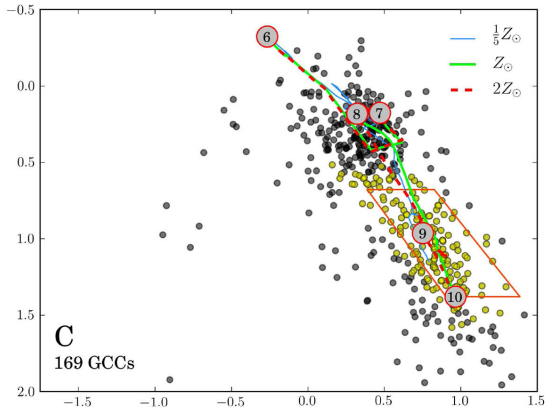

(d)

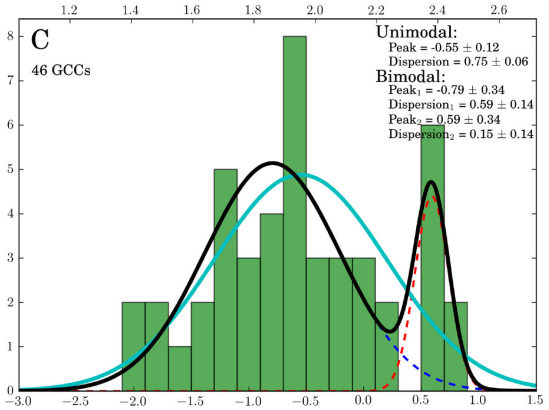

(e)

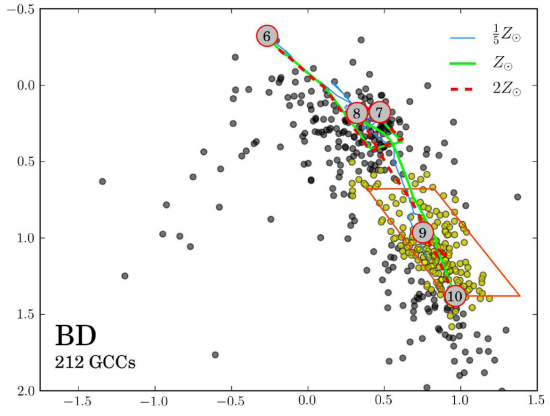

(f)

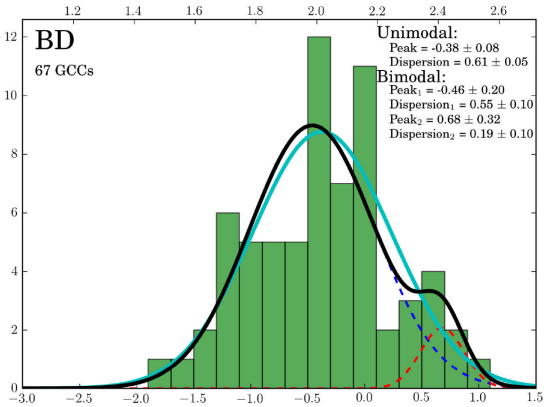

(g)

Figure 15 – *continued*

of Fig. 11). Specifically, all cluster to the left of the 'blue' peak are considered to be relatively metal-poor. Similarly, all clusters rightwards of the 'red' peak are considered relatively metal-rich. The clusters between the peaks are tagged as having an intermediate metallicity content. Thus, the metal-poor clusters have metallicities below −1.04, −1.05, and −0.93 for galaxies HCG 42A, 59B, and 92E, respectively. The metal-rich clusters have metallicities above 0.16, −0.43, and 0.09, for the same galaxies. Accordingly, the intermediate metallicity clusters in these galaxies have metallicities ranging between the values cited above. Then

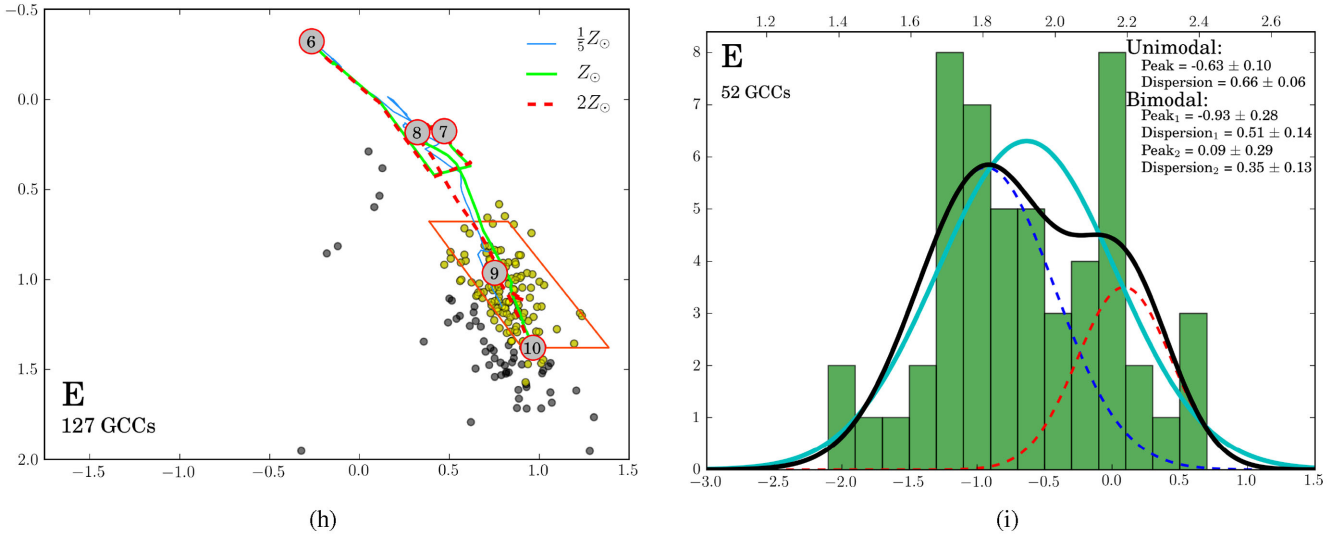

Figure 15 – *continued*

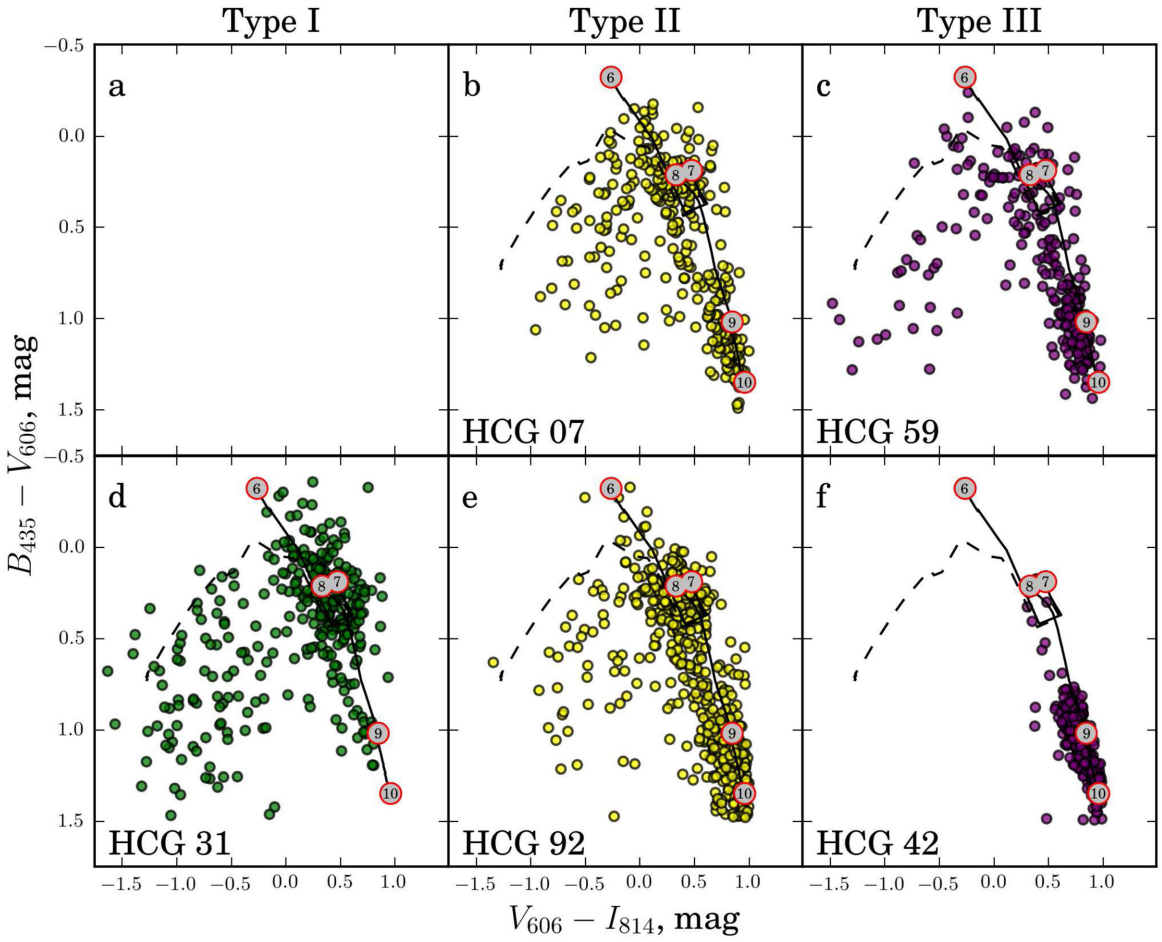

Figure 16. Colour–colour plots of the SCC populations of the CGs in our sample, arranged similarly to fig. 1 in Konstantopoulos et al. (2010). The solid black line traces the evolution of SSP models of 1.0 $Z_\odot$ (Marigo et al. 2008). The dashed line to the left of the main evolutionary track represents a track that incorporates a model of nebular emission (Starburst99; Leitherer et al. 1999), common for young SCs (e.g. Vacca & Conti 1992; Conti, Leitherer & Vacca 1996). The numbers on the track denote age represented in log (age/yr). The upper panels represent groups with the H I gas contained within the member galaxies, whereas the lower panels represent groups with the H I gas stripped from the galaxies. These groups tend to have a rich IGM. Although Konstantopoulos et al. (2013) have classified HCG 59 (panel c) as a Type III group based on its estimated dynamical mass, the SC population is more consistent with a Type II group.

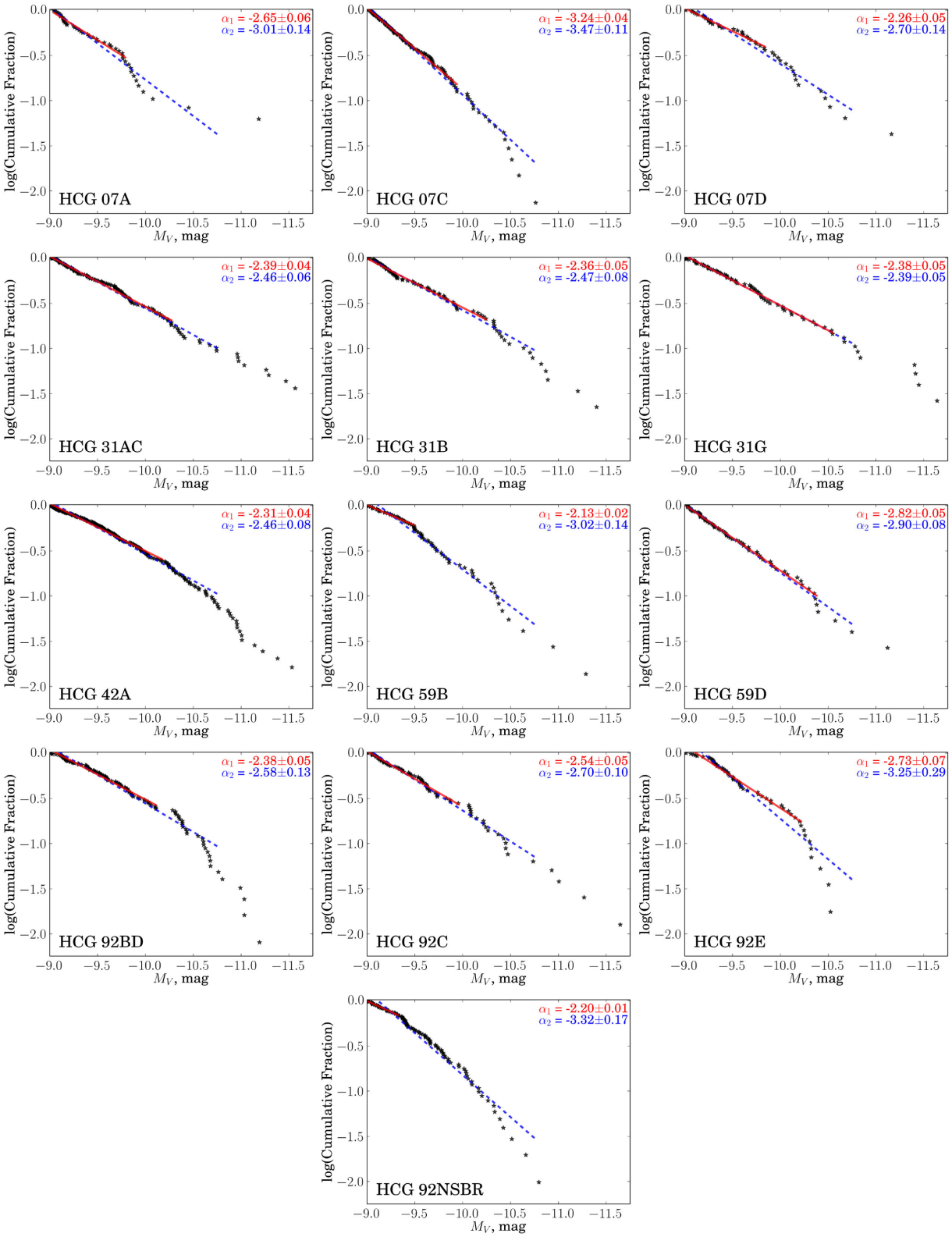

Figure 17. Cumulative luminosity functions of galaxies in our sample. For statistically significant results, only galaxies with more than 40 SCCs were used. The slopes were determined by a least-squares fit over the range covered by the line. The solid line represents the best-fitting slope over the range that was chosen manually, whereas the dashed line represents the best-fitting slope over a common range for all CLFs, from −9 to −10.75 mag. The corresponding α values for each slope are displayed in the upper right corner of each panel.

Table 8. CLF indices for galaxies in our sample that have over 40 SCCs.

Galaxy/Region	N_{SCC}	Type	α-index		Magnitude range	
			α_1	α_2	custom	common
HCG 07A	48	Sb	-2.65 ± 0.06	-3.01 ± 0.14	$-9.00, \ldots, -9.81$	$-9.00, \ldots, -10.75$
HCG 07C	135	SBc	-3.24 ± 0.04	-3.47 ± 0.11	$-9.00, \ldots, -9.96$	
HCG 07D	47	SBc	-2.26 ± 0.05	-2.70 ± 0.14	$-9.00, \ldots, -9.91$	
HCG 31AC	138	Sdm + Im	-2.39 ± 0.04	-2.46 ± 0.06	$-9.00, \ldots, -10.28$	
HCG 31B	89	Sm	-2.36 ± 0.05	-2.47 ± 0.08	$-9.00, \ldots, -10.28$	
HCG 31G	76	Sbc	-2.38 ± 0.05	-2.39 ± 0.05	$-9.00, \ldots, -10.60$	
HCG 42A	246	E3	-2.31 ± 0.04	-2.46 ± 0.08	$-9.00, \ldots, -10.20$	
HCG 59B	73	E0	-2.13 ± 0.02	-3.02 ± 0.14	$-9.00, \ldots, -9.49$	
HCG 59D	75	Im	-2.82 ± 0.05	-2.90 ± 0.08	$-9.00, \ldots, -10.39$	
HCG 92BD	124	Sbc + E2	-2.38 ± 0.05	-2.58 ± 0.13	$-9.00, \ldots, -10.14$	
HCG 92C	79	SBc	-2.54 ± 0.05	-2.70 ± 0.10	$-9.00, \ldots, -10.24$	
HCG 92E	57	E4	-2.73 ± 0.07	-3.25 ± 0.29	$-9.00, \ldots, -9.91$	
HCG 92NSBR	102	–	-2.20 ± 0.01	-3.32 ± 0.17	$-9.00, \ldots, -9.34$	

Notes. Types of galaxies are taken from Hickson et al. (1989). Region 92NSBR represent a collection of intergroup clusters and as such does not have a morphological type. Magnitude range column specifies the range over which the slope was fitted.

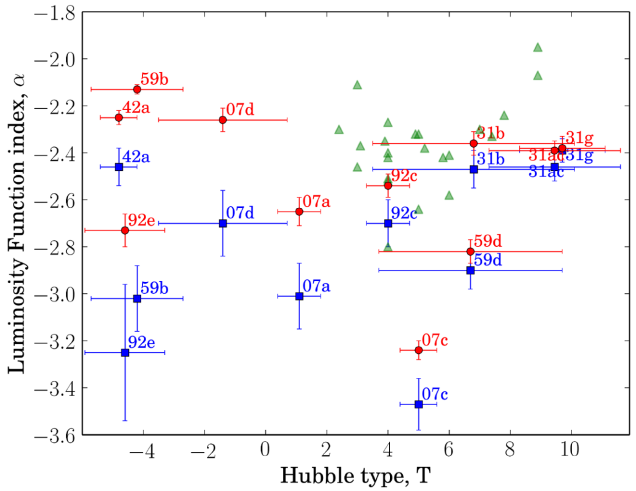

Figure 18. Plot of CLF index α as a function of *Hubble* type (T). Red circles represent indices based on fitting custom ranges of CLFs, and blue squares represent indices of common range fittings. In all cases, extending the fitting range makes the indices more negative. Green triangles are the indices obtained from Whitmore et al. (2014), who studied a sample of 20 nearby star-forming spiral galaxies and found a correlation between α and T, for T ranging from 2 to 9. Based on our sample, it appears that no significant correlation between α and T can be observed. Out of 11 data points in this plot, 1 point does not represent a galaxy itself but rather a pair of close interacting galaxies: 31AC – a combination of spiral and irregular galaxies. Because their *Hubble* type is very close in value (for 31A $T = 8.9 \pm 0.9$, for 31C $T = 10 \pm 2$), for the T value of 31AC we adopted the value of 9.45 ± 2.15. For another interacting pair, 92BD – a close pair of a spiral and an elliptical, the morphological types are very different and the 'average' value would not be meaningful. For this reason, we do not include this data point in our plot. The morphological types are taken from HyperLeda.

we plot the cumulative distribution of the clusters as a function of projected distance from the centre of the galaxy. We find that 42A and 59B have more metal-rich clusters concentrated closer to their galaxy centres, clusters with intermediate metal content are distributed throughout the galaxies, and metal-poor clusters tend to have higher concentrations in the outer regions of the galaxies.

A Kolmogorov–Smirnov (KS) statistical test was used to determine if the cumulative radial distributions of the different metallicity clusters are consistent with each other. The results showed that the p-value for comparing the low and high metallicity distributions in 42A was $\sim 10^{-4}$, which allows us to reject the null hypothesis (that they are drawn from the same parent population) with >99.9 per cent confidence. Similarly, $p = 4 \times 10^{-4}$ for the rich and poor clusters of 59B, and so their radial distributions are also significantly different. For galaxy 92E the p-values for all combinations of distributions are not rejecting the null hypothesis. From the lower panel of Fig. 19, it appears that the GCs of different metallicities are mixed throughout the galaxy. However, we have to note that the statistics of small numbers might be at play here. The way we split the GC population into three groups with the different metallicity content leaves the metal-rich population of 92E with only seven GCs (20 and 26 GCs in metal-poor and medium metal content populations, respectively). Thus, it is highly speculative to talk about the radial distribution of the metal-rich clusters. To try to avoid this situation, we split GC sample into two roughly equal groups, metal-rich and metal-poor, at [Fe/H] = −0.63 (panel i, Fig. 15). The KS test does not reject the null hypothesis, and so it would appear that GCs do not have a preferential distribution based on their metallicities. One of the possible explanations for this apparently well-mixed distribution would be a dry merger between two galaxies of similar mass. An examination of the unsharp-masked image of 92E to look for signs of recent interaction such as shells or streams did not reveal any such features.

5 CONCLUSIONS

We present a catalogue of SCs detected in five compact galaxy groups (HCG 07, HCG 31, HCG 42, HCG 59, and HCG 92), based on sensitive, high-resolution multicolour images from the *Hubble Space Telescope* ACS and WFC3 (in the case of HCG 92) with the goal of examining the properties of the SC systems of CG galaxies overall and further assisting researchers in SC-related studies. Altogether, the catalogue consists of 18 292 objects. After

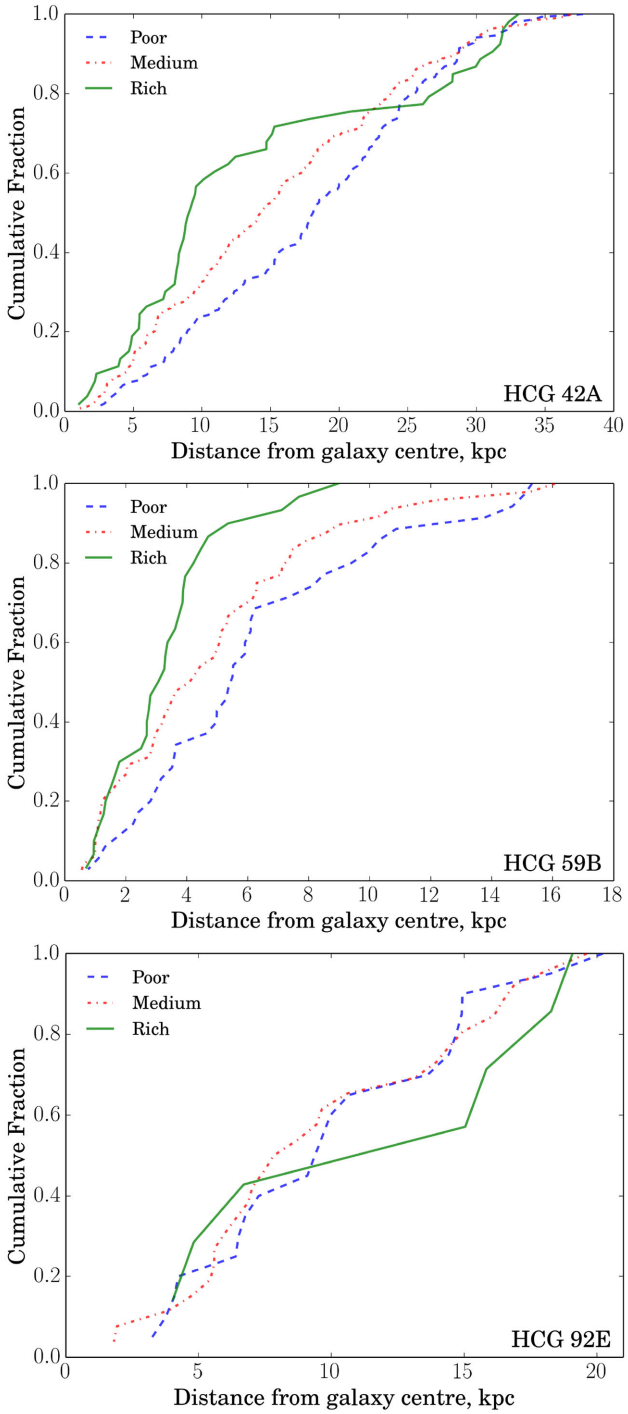

Figure 19. Cumulative function of radial distribution of clusters with different metallicities for galaxies HCG 42A, HCG 59B, and HCG 92E (top, middle, and bottom panels, respectively). The KS-test has shown that metal-rich and metal-poor populations of 42A and 59B are drawn from different distributions (with confidence of >99 per cent). The GC populations in 92E appear to be well mixed throughout the galaxy.

applying a number of criteria, we are left with 1963 SCCs and 1505 GCCs detected in 16 galaxies in the high-confidence samples. A sample of the photometric data from this catalogue is presented in the electronic Table 9.

In particular, a detailed examination of our catalogue revealed the following.

Table 9. A sample table of the *BVI* catalogue for SCs in HCGs. The full catalogue is available online.

RA	Dec.	*B*			*V*			*I*																
(deg)	(deg)	(mag)	err	sharp	(mag)	err	sharp	(mag)	err	sharp	χ_1	S1	S2	S3	S4	S5	G1	G2	G3	G4	SCC	GCC	[Fe/H]	HCG
(1)	(2)	(3)	(4)	(5)	(6)	(7)	(8)	(9)	(10)	(11)	(12)	(13)	(14)	(15)	(16)	(17)	(18)	(19)	(20)	(21)	(22)	(23)	(24)	(25)
338.9945	33.936 701	28.921	0.502	− 0.122	27.844	0.203	− 0.67	26.716	0.107	0.143	1.35	0	0	1	1	0	1	1	0	1	–	–	0.1232	92
339.042 61	33.936 755	25.844	0.057	0.112	25.462	0.048	0.224	24.997	0.055	0.218	1.784	1	1	1	1	1	1	1	1	0	yes	–	− 3.441	92
339.025 44	33.936 792	26.918	0.1	0.111	26.642	0.123	− 0.615	26.429	0.183	− 0.408	2.811	0	1	1	1	1	1	0	1	0	–	–	− 4.399	92
338.963 91	33.936 928	27.076	0.13	− 0.348	25.919	0.062	− 0.079	25.111	0.054	0.075	1.606	0	1	1	1	1	1	1	1	1	–	yes	− 0.499	92
338.977 34	33.937 033	26.903	0.116	0.033	26.369	0.075	− 0.046	25.716	0.158	0.122	3.819	0	1	1	0	1	1	1	1	0	–	–	− 2.539	92
339.0115	33.937 167	28.51	0.365	0.652	27.192	0.105	− 0.22	27.058	0.208	− 0.034	2.137	0	0	1	1	1	1	1	0	0	–	–	− 1.840	92
339.033 73	33.937 201	28.678	0.388	− 1.17	26.171	0.075	0.168	26.308	0.128	0.439	2.171	0	0	1	1	0	1	1	1	0	–	–	0.5495	92
338.958 18	33.937 251	27.208	0.144	− 0.517	26.064	0.066	− 0.137	25.33	0.074	− 0.072	2.078	0	1	1	1	1	1	1	1	1	–	yes	− 0.725	92
339.002 39	33.937 31	26.475	0.063	0.313	25.395	0.057	0.369	24.446	0.063	0.386	2.433	1	1	1	1	1	1	1	1	1	yes	yes	− 0.333	92
338.961 15	33.937 42	25.62	0.046	0.182	24.629	0.026	− 0.035	23.736	0.042	0.19	1.955	1	1	1	1	1	1	1	1	1	yes	yes	− 0.710	92
339.023 47	33.937 46	28.012	0.228	− 1.068	26.94	0.093	0.051	25.747	0.102	0.029	2.271	0	1	1	1	0	1	1	1	1	–	yes	0.2784	92
338.999 22	33.937 483	27.763	0.155	0.289	25.791	0.051	0.236	24.743	0.064	0.337	2.284	0	1	1	1	0	1	1	1	0	–	–	2.2147	92

Notes. Columns list: (1) right ascension (J2000); (2) declination (J2000); (3)–(5) magnitude, error in magnitude, and sharpness values for *B* band (*F435W*; *F438W* for HCG 92); (6)–(8) magnitude, error in magnitude, and sharpness values for *V* band (*F606W*); (9)–(11) magnitude, error in magnitude, and sharpness values for *I* band (*F814W*); (12) goodness of fit factor χ from PSF-fitting in *I* band; (13)–(17) SCCs selection criteria, see Section 3.3 for full description. 1 means that a given criterion is satisfied; (18)–(20) GCC selection criteria, see Section 3.4 for full description. 1 means that given criterion is satisfied; (21) SCC flag. If 'yes', all SCC criteria are satisfied; (22) GCC flag. If 'yes', all GCC criteria are satisfied; (23) Metallicity value derived from $B-I$ colour, see Section 4 for more details; (24) HCG number.

(i) SCs are powerful tracers of episodes of star formation activity. Careful study of the distribution of cluster colours can lead to a better understanding of the evolutionary state of their hosts and can help to constrain (and in some cases to reconstruct) the sequence of events in the host groups (e.g. Gallagher et al. 2010; Konstantopoulos et al. 2010, 2012, 2013; Fedotov et al. 2011). Thus, the analysis of SC populations in CGs allowed us to propose a reclassification of HCG 59 from a Type III to a Type II group. Most galaxies in Type III groups appear to be 'red' and 'dead' (e.g. HCG 42). However, the galaxy morphologies of HCG 59 do not comply with that statement. Moreover, its population of SCs is more consistent with Type II groups.

(ii) In general, the CLFs of the CG spiral galaxies were consistent with spirals studied in the literature (e.g. Larsen 2002; Whitmore et al. 2014). In particular, their CLF α-values ranged from -2.26 ± 0.05 to -2.54 ± 0.05. A notable exception were the large negative α-values for the spirals HCG 07A and HCG 07C with $\alpha = -2.65 \pm 0.06$ and -3.24 ± 0.04, respectively.

(iii) We have examined the metallicity distributions of GCCs in the five groups overall and individually in the elliptical galaxies (nominally elliptical 07BD and 92BD, 42A, 59B, 92C, and 92E) with sufficient numbers of GCCs. Only in galaxy 42A do we detect a metallicity distribution with well-defined bimodality peaking at [Fe/H] $= -1.04 \pm 0.07$ and -0.16 ± 0.15. The galaxy 92C may also host a bimodal distribution, but the statistical results were not conclusive.

(iv) The number of GCs in each galaxy is proportional to the total stellar masses of galaxies (Fig. 4). Notably, we detect a rather large number of GCs in 59B (and its immediate environs) and a small number of GCs in 59A. It is possible that these two galaxies have interacted before given their morphologies (59B is elliptical, 59A is lenticular) and apparent proximity; the GC population distribution may be the only record of that interaction. A low surface brightness stream of material between galaxies 59A and 59B, reported in Konstantopoulos et al. (2013), as well as their line-of-sight velocities (within 3 per cent of each other) also support the idea of previous interactions.

(v) The number of 'blue' clusters (with colour $V - I < 0.1$, representing the population of young SCs) is well correlated with the SFR. Two spiral galaxies (92C and 59C) have a large number of 'blue' clusters given their relatively lower SFRs. That likely indicates that a recent bout of star formation triggered by interactions is coming to an end. However, the young SCs have not been significantly age-dimmed yet, and so a large number of them are still detectable.

(vi) For the three elliptical galaxies in our sample (42A, 59B, and 92E), we looked at the radial distribution of GCs of different metallicities. According to the KS-test, metal-rich and metal-poor populations of 42A and 59B are drawn from different distributions (with confidence of >99 per cent). The GCs of different metallicities in 92E appear to be well mixed throughout the galaxy. Dry mergers of galaxies with a similar mass could explain this last observation. However, the characteristic features for such a merger (such as shells and streams) are not detected.

The SC populations of HCG galaxies are particularly interesting given their potential to reveal the history of dynamical interactions that have clearly been so important in shaping the evolution of individual groups as a whole and the current state of their member galaxies. The sensitive *BVI* imaging and photometry presented in this catalogue illustrate this point. However, the advantage of adding *U* band to photometric studies of SCs is considerable. It breaks the age-extinction degeneracy of the *BVI* photometry and allows a shift from a qualitative description of cluster ages to a more quantitative analysis, along with determinations of intrinsic reddening and masses. This additional information adds considerably to the descriptive power of SC populations in specific environments.

Our future work on SC populations of Stephan's Quintet (HCG 92; Fedotov et al., in preparation) with *UBVI* photometry will illustrate that.

ACKNOWLEDGEMENTS

KF and SCG thank the Natural Sciences and Engineering Research Council of Canada and the Ontario Early Researcher Award Program for support. This research has made use of the NED which is operated by the Jet Propulsion Laboratory, California Institute of Technology, under contract with the National Aeronautics and Space Administration (NASA). Additional support for this work was provided by NASA through grant no. HST-GO-10787.15-A from the Space Telescope Science Institute which is operated by AURA, Inc., under NASA contract NAS 5-26555. We thank Alan McConnachie, John Blakeslee, Pat Côte, and Ruben Sanchez-Janssen for illuminating discussions on the properties of GCs and Peter Stetson for sharing his insight in aperture and PSF photometries. We also thank Theodoros Bitsakis, the referee for this paper, for the supportive encouragement of our work and for suggestions that improved the manuscript. We thank Robert Corless, Gretchen Harris, John Landstreet, and Aaron Sigut for a careful read of the manuscript and their valuable suggestions.

Facilities: HST

REFERENCES

Ashman K. M., Zepf S. E., 1998, Globular Cluster Systems. Cambridge University Press, Cambridge
Barmby P., Huchra J. P., Brodie J. P., Forbes D. A., Schroder L. L., Grillmair C. J., 2000, AJ, 119, 727
Barmby P., Kuntz K. D., Huchra J. P., Brodie J. P., 2006, AJ, 132, 883
Barton Gillespie E., Geller M. J., Kenyon S. J., 2003, ApJ, 582, 668
Bastian N., Gieles M., Lamers H. J. G. L. M., Scheepmaker R. A., de Grijs R., 2005, A&A, 431, 905
Bitsakis T., Charmandaris V., da Cunha E., Díaz-Santos T., Le Floc'h E., Magdis G., 2011, A&A, 533, A142
Bitsakis T., Charmandaris V., Appleton P. N., Díaz-Santos T., Le Floc'h E., da Cunha E., Alatalo K., Cluver M., 2014, A&A, 565, A25
Blakeslee J. P., Cho H., Peng E. W., Ferrarese L., Jordán A., Martel A. R., 2012, ApJ, 746, 88
Bressert E. et al., 2010, MNRAS, 409, L54
Carrasco E. R., Mendes de Oliveira C., Infante L., 2006, AJ, 132, 1796
Chandar R., Whitmore B., Lee M. G., 2004, ApJ, 611, 220
Conti P. S., Leitherer C., Vacca W. D., 1996, ApJ, 461, L87
de Vaucouleurs G., de Vaucouleurs A., Corwin H. G., Jr Buta R. J., Paturel G., Fouqué P., 1991, Third Reference Catalogue of Bright Galaxies. Volume I: Explanations and references. Volume II: Data for galaxies between 0^h and 12^h. Volume III: Data for galaxies between 12^h and 24^h. Springer-Verlag, Berlin
Desjardins T. D. et al., 2014, ApJ, 790, 132
Fedotov K., Gallagher S. C., Konstantopoulos I. S., Chandar R., Bastian N., Charlton J. C., Whitmore B. C., Trancho G., 2011, AJ, 142, 42
Gallagher S. C., Charlton J. C., Hunsberger S. D., Zaritsky D., Whitmore B. C., 2001, AJ, 122, 163
Gallagher S. C. et al., 2010, AJ, 139, 545
Gieles M., Larsen S. S., Bastian N., Stein I. T., 2006, A&A, 450, 129
Goudfrooij P., Strader J., Brenneman L., Kissler-Patig M., Minniti D., Edwin Huizinga J., 2003, MNRAS, 343, 665
Harris W. E., 1996, AJ, 112, 1487

Harris W. E., 2001, in Labhardt L., Binggeli B., eds, Saas-Fee Advanced Course 28: Star Clusters. Springer-Verlag, Berlin, p. 223
Harris W. E., 2009, ApJ, 699, 254
Harris W. E., Whitmore B. C., Karakla D., Oko W., Baum W. A., Hanes D. A., Kavelaars J. J., 2006, ApJ, 636, 90
Harris W. E., Harris G. L. H., Alessi M., 2013, ApJ, 772, 82
Hickson P., 1982, ApJ, 255, 382
Hickson P., 1997, ARA&A, 35, 357
Hickson P., Kindl E., Auman J., 1989, ApJS, 70, 687
Hickson P., Mendes de Oliveira C., Huchra J. P., Palumbo G., 1992, ApJ, 399, 353
Johnson K. E., Hibbard J. E., Gallagher S. C., Charlton J. C., Hornschemeier A. E., Jarrett T. H., Reines A. E., 2007, AJ, 134, 1522
Jones L. R., Ponman T. J., Horton A., Babul A., Ebeling H., Burke D. J., 2003, MNRAS, 343, 627
Kennicutt R. C., Jr, Roettiger K. A., Keel W. C., van der Hulst J. M., Hummel E., 1987, AJ, 93, 1011
Konstantopoulos I. S. et al., 2010, ApJ, 723, 197
Konstantopoulos I. S. et al., 2012, ApJ, 745, 30
Konstantopoulos I. S. et al., 2013, ApJ, 770, 114
Kundu A., Whitmore B. C., 2001, AJ, 122, 1251
Lada C. J., Lada E. A., 2003, ARA&A, 41, 57
Larsen S. S., 2002, AJ, 124, 1393
Larsen S. S., 2004, A&A, 416, 537
Leitherer C. et al., 1999, ApJS, 123, 3
McConnachie A. W., Ellison S. L., Patton D. R., 2008, MNRAS, 387, 1281
Marigo P., Girardi L., Bressan A., Groenewegen M. A. T., Silva L., Granato G. L., 2008, A&A, 482, 883
Makarov D., Prugniel P., Terekhova N., Courtois H., Vauglin I., 2014, A&A, 570, A13
Mendes de Oliveira C. L., Temporin S., Cypriano E. S., Plana H., Amram P., Sodré L., Jr, Balkowski C., 2006, AJ, 132, 570
Mihos J. C., Hernquist L., 1996, ApJ, 464, 641
Misgeld I., Hilker M., 2011, MNRAS, 414, 3699
Moles M., Sulentic J. W., Márquez I., 1997, ApJ, 485, L69
Moles M., Marquez I., Sulentic J. W., 1998, A&A, 334, 8
Mould J. R. et al., 2000, ApJ, 529, 786
Muratov A. L., Gnedin O. Y., 2010, ApJ, 718, 1266
Murdin P., 2001, Encyclopedia of Astronomy and Astrophysics. Nature Publishing, London
Nishiura S., Shimada M., Ohyama Y., Murayama T., Taniguchi Y., 2000, AJ, 120, 1691
Peng E. W. et al., 2006, ApJ, 639, 95
Rejkuba M., Greggio L., Harris W. E., Harris G. L. H., Peng E. W., 2005, ApJ, 631, 262
Rhode K. L., Zepf S. E., Kundu A., Larner A. N., 2007, AJ, 134, 1403
Robin A. C., Reylé C., Derrière S., Picaud S., 2003, A&A, 409, 523
Ryon J. E. et al., 2014, AJ, 148, 33
Sabater J., Verdes-Montenegro L., Leon S., Best P., Sulentic J., 2012, A&A, 545, A15
Scheepmaker R. A., Haas M. R., Gieles M., Bastian N., Larsen S. R. S., Lamers H. J. G. L. M., 2007, A&A, 469, 925
Schlafly E. F., Finkbeiner D. P., 2011, ApJ, 737, 103
Schlegel D. J., Finkbeiner D. P., Davis M., 1998, ApJ, 500, 525
Sirianni M. et al., 2005, PASP, 117, 1049
Springel V., Di Matteo T., Hernquist L., 2005, MNRAS, 361, 776
Stetson P. B., 1987, PASP, 99, 191
Sulentic J. W., Rosado M., Dultzin-Hacyan D., Verdes-Montenegro L., Trinchieri G., Xu C. K., Pietsch W., 2001, AJ, 122, 2993
Temporin S., Staveley-Smith L., Kerber F., 2005, MNRAS, 356, 343
Trancho G., Konstantopoulos I. S., Bastian N., Fedotov K., Gallagher S., Mullan B., Charlton J. C., 2012, ApJ, 748, 102
Tzanavaris P. et al., 2010, ApJ, 716, 556
Vacca W. D., Conti P. S., 1992, ApJ, 401, 543
VanDalfsen M. L., Harris W. E., 2004, AJ, 127, 368
Verdes-Montenegro L., Yun M. S., Williams B. A., Huchtmeier W. K., Del Olmo A., Perea J., 2001, A&A, 377, 812
Whitmore B. C., Zhang Q., 2002, AJ, 124, 1418
Whitmore B. C., Zhang Q., Leitherer C., Fall S. M., Schweizer F., Miller B. W., 1999, AJ, 118, 1551
Whitmore B. C., Chandar R., Bowers A. S., Larsen S., Lindsay K., Ansari A., Evans J., 2014, AJ, 147, 78
Wilson C. D., Harris W. E., Longden R., Scoville N. Z., 2006, ApJ, 641, 763
Xu C. K., Sulentic J. W., Tuffs R., 1999, ApJ, 512, 178
York D. G. et al., 2005, in Williams P., Shu C.-G., Menard B., eds, IAU Colloq. 199: Probing Galaxies through Quasar Absorption Lines. Cambridge University Press, Cambridge, p. 58

SUPPORTING INFORMATION

Additional Supporting Information may be found in the online version of this article:

Table 9. A sample table of the *BVI* catalogue for SCs in HCGs (http://mnras.oxfordjournals.org/lookup/suppl/doi:10.1093/mnras/stv349/-/DC1).

Please note: Oxford University Press are not responsible for the content or functionality of any supporting materials supplied by the authors. Any queries (other than missing material) should be directed to the corresponding author for the paper.

This paper has been typeset from a TEX/LATEX file prepared by the author.